

# Rotation Equivariant Mamba for Vision Tasks

Zhongchen Zhao, Qi Xie, Keyu Huang, Lei Zhang, Deyu Meng, and Zongben Xu

**Abstract**—Rotation equivariance constitutes one of the most general and crucial structural priors for visual data, yet it remains notably absent from current Mamba-based vision architectures. Despite the success of Mamba in natural language processing and its growing adoption in computer vision, existing visual Mamba models fail to account for rotational symmetry in their design. This omission renders them inherently sensitive to image rotations, thereby constraining their robustness and cross-task generalization. To address this limitation, we propose to incorporate rotation symmetry, a universal and fundamental geometric prior in images, into Mamba-based architectures. Specifically, we introduce EQ-VMamba, the first rotation equivariant visual Mamba architecture for vision tasks. The core components of EQ-VMamba include a carefully designed rotation equivariant cross-scan strategy and group Mamba blocks. Moreover, we provide a rigorous theoretical analysis of the intrinsic equivariance error, demonstrating that the proposed architecture enforces end-to-end rotation equivariance throughout the network. Extensive experiments across multiple benchmarks—including high-level image classification task, mid-level semantic segmentation task, and low-level image super-resolution task—demonstrate that EQ-VMamba achieves superior or competitive performance compared to non-equivariant baselines, while requiring approximately 50% fewer parameters. These results indicate that embedding rotation equivariance not only effectively bolsters the robustness of visual Mamba models against rotation transformations, but also enhances overall performance with significantly improved parameter efficiency. Code is available at <https://github.com/zhongchenzhao/EQ-VMamba>.

**Index Terms**—Rotation equivariant Mamba, equivariant networks, visual Mamba, state space models.

## I. INTRODUCTION

IN recent years, Mamba [1] has emerged as one of the most promising next-generation foundational architectures in deep learning, succeeding convolutional neural networks (CNNs) [2]–[6] and Transformers [7]–[9]. In contrast to Transformers, which suffer from quadratic computational complexity, Mamba inherits the core paradigm of State Space Models (SSMs) [10]–[12] to maintain linear complexity. Building on this, it employs a more powerful selective scan mechanism for long-range dependency modeling. Leveraging these advantages, Mamba represents the first linear-complexity architecture to achieve performance comparable to Transformers in natural language processing (NLP).

Following Mamba’s success in NLP, numerous studies [13]–[17] have explored its adaptation to the visual domain. For instance, Vim [13] directly replaces the self-attention mechanism in Transformers with a bidirectional Mamba block,

Zhongchen Zhao, Qi Xie, Keyu Huang, Deyu Meng, and Zongben Xu are with the School of Mathematics and Statistics, Xi’an Jiaotong University, Shaanxi, P.R.China (e-mail: zhongchenzhao@stu.xjtu.edu.cn, xie.qi, keyu.huang, dymeng, zbxu@mail.xjtu.edu.cn).

Lei Zhang is with the Department of Computing, the Hong Kong Polytechnic University, Hong Kong, P.R.China (e-mail: cslzhang@comp.polyu.edu).

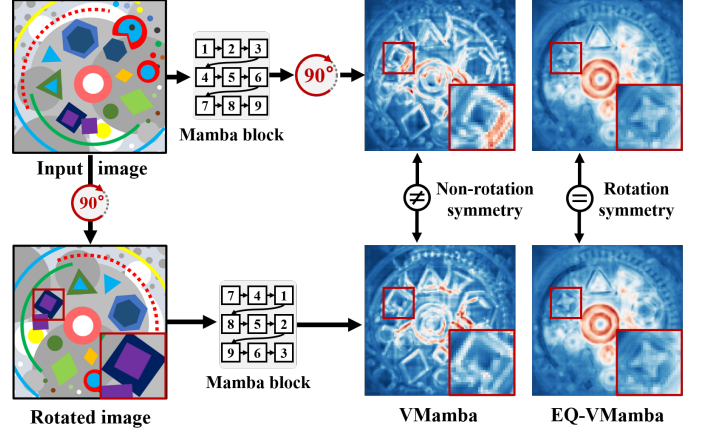


Fig. 1. Visualization of output feature maps for an input image and its rotated version, comparing standard VMamba with our proposed EQ-VMamba.

providing the first validation of Mamba’s feasibility in vision applications. To address the structural discrepancy between 2D image tokens and 1D textual sequences, VMamba [14] introduces a Visual State-Space (VSS) block with a cross-scan strategy, enabling each token to symmetrically integrate global information from four directions in the 2D plane. Building on this, VMamba outperforms Swin Transformer [9] on high-level vision tasks, highlighting the potential of Mamba-based architectures in vision domain. Subsequently, MambaIR [17] extends the cross-scan strategy to low-level vision tasks, proposing the first Mamba-based model for image restoration and achieving competitive or superior results compared to state-of-the-art Transformer-based models.

However, the direct adaptation of Mamba from NLP to vision often yields suboptimal performance due to cross-modal discrepancies. Current studies, represented by VMamba [14], primarily focus on bridging the structural gaps between images and languages, while largely overlooking the fundamental discrepancies in intrinsic content properties. Unlike textual data, natural images possess pronounced geometric symmetries: identical or similar patterns recur across various positions, orientations, and poses in the image [18]. Neglecting these symmetries increases the learning burden, making models susceptible to overfitting task-irrelevant features and compromising their generalization and robustness.

Previous work [19]–[34] has demonstrated that incorporating geometric symmetry priors into neural networks can significantly enhance model’s generalization and robustness. Specifically, the geometric symmetry prior of images implies that the network’s prediction for a transformed image (e.g., translation, rotation, or reflection) should be consistent with the transformation applied to the network’s prediction of the original image. Fundamental architectures such as CNNs and ViTs inherently possess a certain degree of equivariance. For instance, CNNs explicitly embed translation equivariance

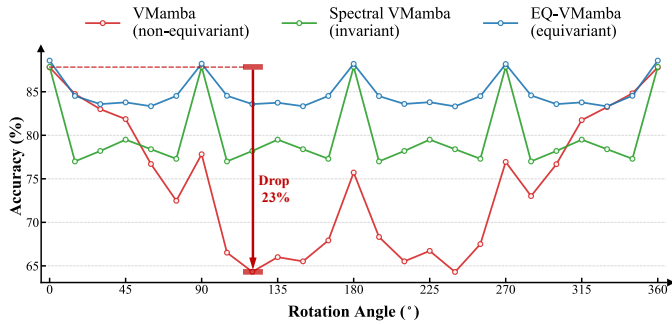


Fig. 2. Robustness comparison between VMamba, Spectral VMamba, and EQ-VMamba on the rotated ImageNet-100 dataset.

through sliding convolution kernels, while rotation equivariant CNNs [19], [20] extend this by sharing kernels across an additional group dimension, reducing parameters while bolstering generalization. Furthermore, recent studies [23]–[25], [31], [35] reveal that the self-attention mechanism in ViTs exhibits inherent translation, rotation, and reflection equivariances. These desirable properties enable it to avoid interference from redundant spatial transformations and efficiently extract meaningful features from images.

Compared to the self-attention mechanism in ViTs, the core Visual State-Space (VSS) block in VMamba inherently lacks rotation equivariance. Although the VSS block employs a four-way scanning mechanism to traverse 2D image tokens, rotational transformations of the image still undesirably alter the scanning order, rendering the model highly sensitive to such transformations. As shown in Fig. 1, for the same image at different rotation angles, VMamba produces completely different outputs, leading to significant performance degradation (as shown in Fig. 2 and Tab. III). Furthermore, the lack of rotation equivariance disrupts the rotational symmetry of local structures within an image. Therefore, constructing a rotation equivariant VMamba is of great importance to enhance the model’s generalization, robustness, and parameter efficiency.

However, designing a strictly rotation equivariant VMamba presents several non-trivial challenges. Specifically, to guarantee end-to-end rotation equivariance, each module within the architecture must satisfy the equivariance constraint. This requires: 1) a redesigned rotation equivariant scanning mechanism tailored for 2D images; 2) reformulating Mamba block parameters to preserve equivariance throughout the state-space transformation; 3) adapting non-equivariant modules - such as depthwise convolutions, downsampling layers, and task-specific decoders - to be rotation equivariant.

To address these challenges, we propose EQ-VMamba, a strictly 90-degree rotation equivariant visual Mamba architecture which effectively alleviates the poor robustness of VMamba to image rotations. To the best of our knowledge, this is the first work to extend rotation equivariant design from CNN- and Transformer-based architectures to the emerging Mamba-based architecture, thereby enriching the existing framework of equivariant neural networks. Specifically, the main contributions of this paper are summarized as follows:

- **Model Architecture:** We present the first rigorous formulation for designing a 90-degree rotation-equivariant Mamba architecture. Specifically, we propose a rotation-

equivariant cross-scan (EQ-cross-scan) strategy that employs four symmetric scanning routes to independently process the rotation group components of the feature map. Furthermore, we reformulate the Mamba parameters (e.g.,  $A, B, C, D, \Delta$ ) to construct the rotation equivariant group Mamba blocks. Building on this, we construct an equivariant Visual State-Space (EQ-VSS) block and adapt VMamba and MambaIR, two representative models for high-level and low-level vision tasks, into their equivariant counterparts: EQ-VMamba and EQ-MambaIR.

- **Parameter Efficiency:** Through careful architectural design, EQ-VMamba maintains a computational complexity comparable to its non-equivariant counterparts. Furthermore, by sharing parameters across the group dimension, our approach reduces the total number of learnable parameters by approximately 50%, significantly enhancing parameter utilization efficiency.
- **Theoretical Analysis:** We provide a comprehensive theoretical foundation for the proposed EQ-VMamba architecture. Through the equivariance error analysis, we prove that the proposed EQ-cross-scan, the group Mamba blocks, and the overall EQ-VMamba architecture achieve zero error under 90-degree rotations.
- **Empirical Validation:** Extensive experiments across image classification, semantic segmentation, and super-resolution demonstrate that EQ-VMamba and EQ-MambaIR consistently outperform their non-equivariant counterparts. Evaluations on rotated benchmarks confirm that EQ-VMamba successfully addresses the rotational robustness bottlenecks of the original architecture. Collectively, these results demonstrate that incorporating rotation equivariance into the Mamba framework not only significantly enhances robustness against rotation transformations but also improves overall performance.

The remainder of this paper is organized as follows. Sec. II reviews related work. Sec. III details the proposed rotation equivariant visual Mamba in detail, together with theoretical analyses of its equivariance error. Sec. IV presents extensive experimental results across multiple vision tasks to evaluate the proposed method. Finally, Sec. V concludes the paper and discusses future research directions.

## II. RELATED WORK

### A. Visual Mamba

As the dominant foundational architecture in deep learning, Transformer [7] is primarily constrained by the quadratic complexity of its self-attention mechanism, which scales quadratically with the input sequence length. This computational bottleneck severely restricts its efficiency in processing long-range dependencies. In recent years, numerous sub-quadratic architectures—such as linear attention [36], sparse Transformers [37], and various recurrent neural networks (e.g., LSTM [38], RWKV [39] and RetNet [40])—have been proposed to alleviate this issue. However, these alternatives often struggle to achieve an optimal balance between computational efficiency and model performance.

Recently, Mamba [1], a representative state space model (SSM), has for the first time achieved Transformer-level performance on NLP tasks while maintaining linear-time complexity, marking a significant milestone in the field. Specifically, Mamba inherits the recurrent propagation mechanism of SSMs [10]–[12] for linear-time sequence modeling, and further introduces a powerful input-dependent selective scan mechanism, allowing the model to selectively propagate or forget history information along the scanning sequence. Given its efficiency and efficacy, Mamba has emerged as a promising alternative to Transformers, attracting significant attention from the research community.

Inspired by Mamba’s success in NLP, numerous studies [13]–[16], [41]–[43] have explored its potential for vision tasks. For example, Vim [13] pioneered this by replacing the original unidirectional scanning strategy with a bidirectional scanning strategy tailored for images. Subsequently, VMamba [14] identified that the 1D scanning strategy originally designed for text sequences in Mamba is ill-suited to the 2D structure of images and proposed a cross-scan strategy (i.e., a four-way scanning mechanism) to integrate global information from four directions. With a series of architectural enhancements, VMamba achieves superior performance on high-level vision tasks, surpassing Swin Transformer [9] in both accuracy and inference throughput.

Beyond mainstream high-level vision tasks, Mamba has been extended to a broader range of visual domains, including image restoration [17], [44], [45], image generation [46], video analysis [47], remote sensing images [48], [49], point cloud analysis [50], [51], and medical image analysis [52]. For example, MambaIR [17] introduced the first Mamba-based framework for image restoration, utilizing the cross-scan strategy from VMamba to enhance local features with a global receptive field, while incorporating channel attention mechanisms to reduce channel redundancy. Extensive experiments on various image restoration benchmarks demonstrate that MambaIR achieves competitive or superior performance compared to many well-established CNN- and Transformer-based methods [53], [54].

Although the significant potential of Mamba-based architectures in the visual domain has been demonstrated, visual Mamba still suffers from a significant limitation: poor robustness to rotation transformations of input images. To address this deficiency, we develop EQ-VMamba by explicitly embedding rotation equivariance into the Mamba architecture.

### B. Rotation Equivariant Neural Networks

Research on rotation symmetry priors has long been an important topic in deep learning. Over the past few years, numerous studies [19]–[34] have attempted to explicitly or implicitly incorporate the rotation symmetry prior into various network architectures. Early attempts [27], [29], [55], [56] primarily relied on data augmentation [57] and regularization to implicitly enforce rotation equivariance. However, these methods suffer from a lack of theoretical guarantees and often exhibit unstable performance in maintaining strict equivariance [32].

Recent works [19]–[22], [30], [32], [58], [59] have focused more on the design of rotation equivariant neural networks that explicitly embed rotation equivariance. For example, G-CNN [19] was the first to successfully establish the group-equivariant convolutional framework, achieving  $\pi/2$  rotation equivariance with rigorous theoretical guarantees. Building on the group convolution, SFCNNs [30] and E2-CNN [20] utilized the filter parametrization technique for arbitrarily-degree equivariance in the continuous domain. Subsequently, PDO-eConvs [21] and PDO-eS2CNNs [59] introduced equivariance error analysis for group equivariant convolutions for the first time, providing further theoretical support. Furthermore, F-Conv [22] leveraged Fourier series expansion to achieve high-accuracy filter-parameterized equivariant convolutions, achieving evidently better performance than classical non-equivariant CNNs on image super-resolution tasks.

Beyond convolutions, B-Conv [32] introduced a rotation equivariant linear layer for multilayer perceptrons (MLPs), constructing a rotation equivariant implicit neural representation framework for arbitrary-scale image super-resolution. For Transformer-based architectures, studies [23]–[25], [31], [35] have demonstrated that the core self-attention mechanism in ViTs possesses inherent rotational properties, leading to the design of equivariant ViTs.

Despite these developments, the research on rotation equivariant Mamba-based architecture remains largely unexplored. While the recent Spectral VMamba [34] utilized a rotation-invariant scanning strategy generated by spectral decomposition for rotation invariance, it suffers from two major drawbacks. First, this approach, which lacks the rotational group dimension, achieves only rotation *invariance* rather than *equivariance*, discarding essential orientation information and thereby limiting its efficacy in mid-level and low-level vision tasks. Second, the reliance on spectral decomposition introduces significant computational overhead. In contrast, our proposed EQ-VMamba is a group-based equivariant architecture that preserves the orientation information of local patches. Moreover, the proposed EQ-cross-scan strategy is simple and efficient, ensuring strict symmetry without incurring additional computational cost.

## III. ROTATION EQUIVARIANT VISUAL MAMBA

In this section, we present a principled framework for the design of EQ-VMamba, a Mamba-based architecture with strict 90-degree ( $p4$  group) rotation equivariance. Beyond the  $p4$  group, our formulation is inherently extensible to finer geometric transformations, such as 45-degree rotations and reflectional symmetries, providing a generalized foundation for equivariant state-space modeling.

The remainder of this section is organized as follows. First, we establish the necessary preliminaries regarding the standard Mamba architecture and the fundamentals of rotation equivariant convolutions. Second, we provide a detailed exposition of the EQ-VMamba architecture, including: 1) the overall architecture; 2) the design of equivariant modules, including the EQ-patch embedding, the EQ-cross-scan strategy, and group Mamba blocks; 3) a rigorous theoretical equivariance analysis

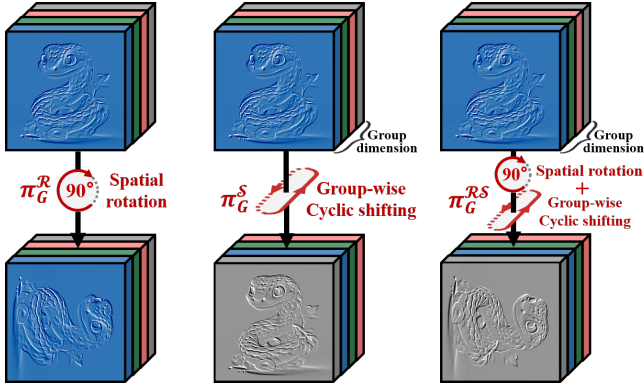


Fig. 3. Illustration of the three fundamental transformation operators utilized within our equivariant framework.

for both the proposed individual modules and entire network; Finally, we introduce two representative mamba-based instantiations—EQ-VMamba and EQ-MambaR—to demonstrate the framework’s versatility across high-level, mid-level, and low-level vision tasks.

#### A. Preliminaries

**Formulation of Mamba.** Mamba [1] extends structured state space sequence models (S4) [11] by introducing a selective mechanism into the recurrent state propagation. Specifically, Mamba maps an input sequence  $\mathbf{x} \in \mathbb{R}^{L1}$  to an output sequence  $\mathbf{y} \in \mathbb{R}^L$  by maintaining a hidden state  $\mathbf{h}_i \in \mathbb{R}^N$ , which is updated via an input-dependent state transition matrix  $\mathbf{A}_i \in \mathbb{R}^{N \times N}$  as follows:

$$\begin{aligned} \mathbf{h}_i &= \mathbf{A}_i \mathbf{h}_{i-1} + \mathbf{B}_i x_i, \\ \mathbf{y}_i &= \mathbf{C}_i^\top \mathbf{h}_i + D x_i, \end{aligned} \quad (1)$$

where  $\mathbf{A}_i$  is a diagonal matrix with elements bounded in  $(0, 1]$ ,  $\mathbf{B}_i, \mathbf{C}_i \in \mathbb{R}^N$  are input-dependent parameters generated by linear projections, and  $D \in \mathbb{R}$  denotes a skip-connection coefficient.  $L$  and  $N$  represent the sequence length and hidden state dimension, respectively. The selective nature of  $\mathbf{A}_i$  enables the model to dynamically propagate or forget historical information, significantly enhancing its capability for long-range dependency modeling.

**Definition of Rotation Equivariance.** Rotation equivariance dictates that a rotation transformation applied to the input results in a predictable, corresponding transformation of the output, preserving the structural relationship between features.

Formally, let  $\Psi$  be a mapping from an input space to an output space, and  $\mathcal{G}$  be a group of rotation transformations defined as:

$$\mathcal{G} = \left\{ G_t = \begin{bmatrix} \cos 2\pi t/T & \sin 2\pi t/T \\ -\sin 2\pi t/T & \cos 2\pi t/T \end{bmatrix} \middle| t=0, 1, \dots, T-1 \right\}. \quad (2)$$

The mapping  $\Psi(\cdot)$  is equivariant with respect to  $\mathcal{G}$  if, for any rotation matrix  $G \in \mathcal{G}$ , it satisfies:

$$\Psi[\pi_G^{\mathcal{R}}(\mathbf{I})] = \tilde{\pi}_G^{\mathcal{R}}[\Psi(\mathbf{I})], \quad (3)$$

<sup>1</sup>For a multi-channel input sequence  $\mathbf{x} \in \mathbb{R}^{L \times C}$ , Mamba processes each channel independently and in parallel.

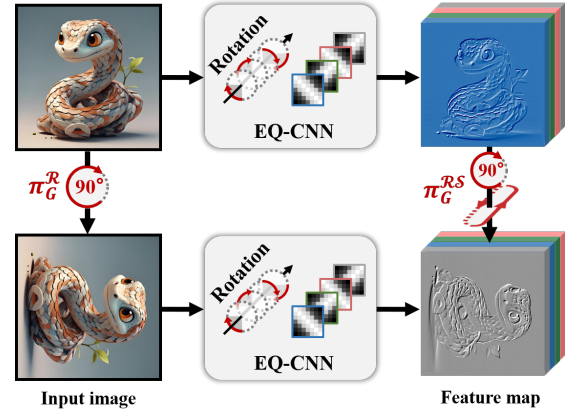


Fig. 4. Illustration of the equivariant property in an EQ-CNN layer. A spatial rotation applied to the input image induces a joint transformation on the output feature map: a corresponding spatial rotation and a cyclic shifting across the rotation group dimension.

where  $\pi_G^{\mathcal{R}}(\cdot)$  denotes the spatial rotation transformation  $G$  acting on the input  $\mathbf{I}$ , and  $\tilde{\pi}_G^{\mathcal{R}}(\cdot)$  denotes the induced transformation on the output  $\Psi(\mathbf{I})$ . Notation  $[\cdot]$  denotes the function composition.

**Rotation Equivariant CNNs.** Classical CNNs achieve translation equivariance by sharing kernels across spatial translations. Analogously, rotation equivariant CNNs (EQ-CNNs) [21], [22], [30] extend this principle by further sharing kernels across discrete spatial rotations. Specifically, as illustrated in Fig. 4, the convolutional kernel  $\mathbf{W}_\Psi \in \mathbb{R}^{K \times K \times C_0 \times C_1 \times T}$  of a EQ-CNN layer  $\Psi(\cdot)$  is defined over an additional rotation group dimension, where the base kernel  $\mathbf{W}_\Psi^{G_0}$ <sup>2</sup> is rotationally replicated  $T$  times according to a discrete rotation group  $\mathcal{G}$ . Formally, given a learnable parameter  $\mathbf{W}_\Psi^{G_0} \in \mathbb{R}^{K \times K \times C_0 \times C_1}$ , the kernel  $\mathbf{W}_\Psi$  is formulated as:

$$\mathbf{W}_\Psi = [\mathbf{W}_\Psi^{G_t} | t=0, 1, \dots, T-1], \quad \mathbf{W}_\Psi^{G_t} = \pi_{G_t}^{\mathcal{R}}(\mathbf{W}_\Psi^{G_0}), \quad (4)$$

where  $\pi_{G_t}^{\mathcal{R}}(\cdot)$  denotes the rotation operator acting on the spatial dimensions of  $\mathbf{W}_\Psi^{G_0}$  associated with  $G_t$ . Accordingly, for an input image  $\mathbf{I} \in \mathbb{R}^{H \times W \times C_0}$ , the EQ-CNN layer  $\Psi(\cdot)$  maps it to a feature map  $\mathbf{X} \in \mathbb{R}^{H \times W \times C_1 \times T^3}$ , which likewise incorporates a rotation group dimension:

$$\mathbf{X} = \Psi(\mathbf{I}) = [\mathbf{X}^{G_t} | t=0, 1, \dots, T-1], \quad \mathbf{X}^{G_t} = \mathbf{W}_\Psi^{G_t} * \mathbf{I}, \quad (5)$$

where  $*$  denotes convolution operation. Under this formulation, the EQ-CNN layer  $\Psi(\cdot)$  satisfies rotation equivariance defined in Eq. 3.

**Rotation Equivariant Linear.** Standard Linear layers (i.e., fully connected layers) typically operate on the channel dimension of feature maps, which is orthogonal to the rotations on spatial dimension. Consequently, a rotation equivariant Linear (EQ-Linear) [32], [60] only needs to preserve the group-wise cyclic shifting induced by rotations. Specifically, given group-structured input feature maps  $\mathbf{X} \in \mathbb{R}^{H \times W \times C_1 \times T}$ , the EQ-

<sup>2</sup>Following the previous work [21], we denote the  $t$ -th group component of the tensor  $\mathbf{W}_\Psi$  as  $\mathbf{W}_\Psi^{G_t}$ , where  $G_t \in \mathcal{G}$  is a rotation matrix that also serves as an index for the rotation mode in  $\mathbf{W}_\Psi$ .

<sup>3</sup>Without loss of generality, we assume a unit stride for  $\Psi(\cdot)$  such that  $\mathbf{X}$  preserves the spatial resolution of the input.

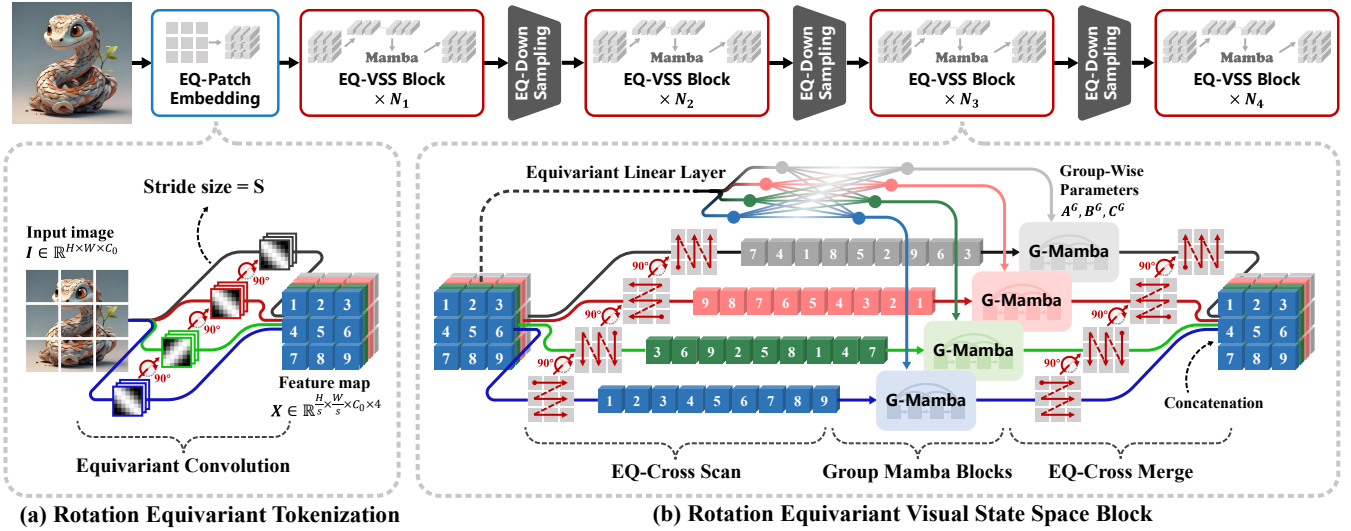


Fig. 5. The overall architecture of the proposed end-to-end rotation equivariant visual Mamba (EQ-VMamba). The framework mainly consists of: (a) an EQ-Patch Embedding module that tokenizes the input image into the group-structured feature maps, and (b) a stack of EQ-VSS blocks for hierarchical feature extraction. Each EQ-VSS block integrates an EQ-cross-scan operation for image-to-sequence flattening, group Mamba blocks for sequence modeling, and an EQ-cross-merge operation for sequence-to-image restoration.

Linear  $\Upsilon(\cdot)$  maps it to output feature maps  $\hat{X} \in \mathbb{R}^{H \times W \times C_2 \times T}$  according to:

$$\begin{aligned} \hat{X} &= \Upsilon(X) = [\hat{X}^{G_t} | t=0, 1, \dots, T-1], \\ \hat{X}^{G_t} &= X \times \pi_{G_t}^S(W_\Upsilon) + b_\Upsilon, \end{aligned} \quad (6)$$

where the learnable parameters  $W_\Upsilon \in \mathbb{R}^{C_1 \times T \times C_2}$  and  $b_\Upsilon \in \mathbb{R}^{C_2}$  denote the weight and bias of  $\Upsilon(\cdot)$ , respectively. Here,  $\pi_{G_t}^S(\cdot)$  denotes  $t$  times cyclic shifting along the rotation group dimension of  $W_\Upsilon$ . Under this formulation, the EQ-Linear layer  $\Upsilon(\cdot)$  satisfies the rotation equivariance defined in Eq. 3.

### B. Overall Architecture of EQ-VMamba

To construct an end-to-end rotation equivariant visual Mamba architecture, each constituent module must strictly satisfy the equivariance constraint defined in Eq. 3. Driven by this requirement, we adopt VMamba [14]—one of the most representative visual Mamba backbones—as our baseline. By reformulating all non-equivariant components into their rotation-equivariant counterparts, we construct the EQ-VMamba architecture. The overall architecture of the EQ-VMamba backbone is illustrated in Fig. 5. Specifically, it consists of the following key equivariant modules:

**Rotation Equivariant Patch Embedding.** The vanilla VMamba begins with a patch embedding layer that partitions the input image into patches and tokenizes them into an initial feature map. However, this standard patch embedding module lacks rotation equivariance. To address this, we develop a rotation equivariant patch embedding that explicitly encodes the orientation information of each patch into the rotation group dimension of the feature map.

**Rotation Equivariant Visual State-Space Block.** Following patch embedding, VMamba utilizes a stack of multiple Visual State-Space (VSS) blocks for hierarchical feature extraction. Each standard VSS block consists of three stages: 1) flattening the 2D feature map into four 1D sequences via the cross-scan mechanism; 2) modeling these sequences with

four independent Mamba blocks; and 3) reconstructing the 2D feature map from output sequences via cross-merge (i.e., the inverse operation of cross-scan). However, both the cross-scan/merge operations and the independent Mamba blocks lack rotation equivariance.

To address this, we propose the rotation equivariant cross-scan/merge to ensure equivariance during the flattening and reconstruction stages. Furthermore, we introduce the group Mamba blocks to ensure rotation equivariance during the sequence modeling stage. By integrating these components, we construct a rotation equivariant EQ-VSS block.

Beyond the primary patch embedding and EQ-VSS blocks, other essential components within VMamba—such as depth-wise convolution and down/up-sampling—also require equivariant modifications to ensure rotation equivariance throughout the network. Fortunately, rotation equivariant versions [20] of these modules are readily available and can be directly substituted into the architecture. By replacing all non-equivariant components with their equivariant counterparts, we obtain an end-to-end rotation equivariant Mamba-based architecture that maintains the original Mamba’s efficiency while significantly enhancing its robustness to rotation transformations.

### C. Rotation Equivariant Tokenization

The vanilla patch embedding in VMamba employs overlapping strided convolutional layers followed by the Layer-Norm2d for tokenization. However, the standard patch embedding is not rotation equivariant, discarding the orientation information of the input image patches.

To address this limitation, we develop a rotation-equivariant patch embedding (EQ-Patch Embedding) by substituting the standard convolutional layers with the EQ-CNN layers [22] defined in Eq. 5. As illustrated in Fig. 6, when the input image undergoes a rotation, the global transformation of the patch grid induces a corresponding spatial rotation on the feature map. Moreover, each patch itself will undergo an intrinsic

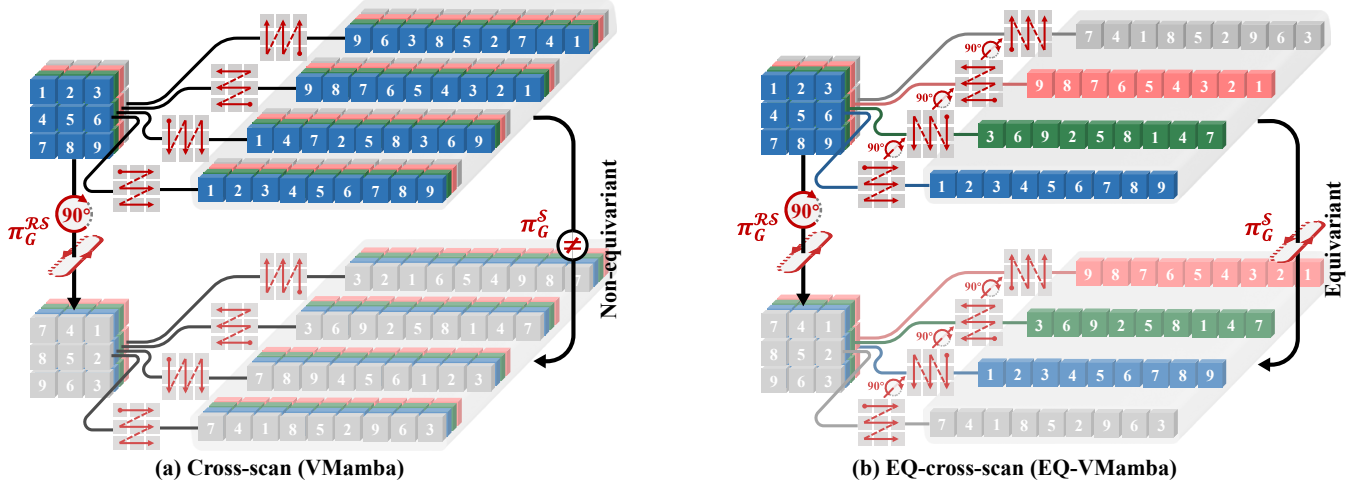


Fig. 6. Comparison between the non-equivariant Cross-Scan and the proposed equivariant EQ-Cross-Scan. (a) Under a  $90^\circ$  rotation of the input image, the standard Cross-Scan fails to maintain sequence consistency. (b) Conversely, EQ-Cross-Scan preserves the ordering of tokens within each 1D sequence, ensuring rigorous structural correspondence between the rotated and unrotated representations.

rotation, inducing a group-wise cyclic shifting on the feature map. Formally, for an input image  $\mathbf{I} \in \mathbb{R}^{H \times W \times C_0}$ , the EQ-CNN layer  $\Psi(\cdot)$  maps it to a group-structured feature map  $\mathbf{X} \in \mathbb{R}^{\frac{H}{s} \times \frac{W}{s} \times C_1 \times 4}$ , where  $s$  denotes the stride size. And for any  $G \in \mathcal{G}$ , we have

$$\begin{aligned} \Psi[\pi_G^{\mathcal{R}}(\mathbf{I})] &= \pi_G^{\mathcal{R}S}[\Psi(\mathbf{I})] = \pi_G^{\mathcal{R}S}(\mathbf{X}) \\ &= \left[ \pi_G^{\mathcal{R}}(\mathbf{X}^{G^{-1}}), \pi_G^{\mathcal{R}}(\mathbf{X}^{G^{-1}G_1}), \dots, \pi_G^{\mathcal{R}}(\mathbf{X}^{G^{-1}G_{T-1}}) \right], \end{aligned} \quad (7)$$

where the operator  $\pi_G^{\mathcal{R}S}(\cdot)$  represents a **\*\*joint transformation\*\*** including both spatial rotation and group-wise cyclic shifting. Consequently, the EQ-Patch Embedding ensures rotation equivariance throughout the tokenization process.

#### D. Rotation Equivariant Visual State-Space Block

The core contribution of EQ-VMamba is the design of a rotation equivariant Visual State-Space (EQ-VSS) block, which primarily incorporates a novel rotation equivariant cross-scan/merge strategy and group Mamba blocks.

**Rotation Equivariant Cross-Scan/Merge.** As formulated in Eq 1, Mamba is inherently designed for processing one-dimensional sequential data. To apply this mechanism to 2D image data, VMamba employs a four-way cross-scan strategy that flattens 2D image tokens into four distinct 1D sequences. However, this vanilla cross-scan strategy fails to satisfy rotation equivariance. As illustrated in Fig. 6 (a), a rotation of the input image induces inconsistent and misaligned transformations on the resulting sequences. Furthermore, unlike learnable parameters in CNNs or MLPs, which can approximate or achieve rotation equivariance through gradient-based optimization, the predefined and fixed cross-scan in VMamba fundamentally prevents the model from learning rotation equivariant representations.

To achieve rigorous equivariance, we propose a simple yet effective rotation equivariant cross-scan (EQ-cross-scan) strategy for image-to-sequence flattening. As illustrated in Fig. 6 (b), the proposed EQ cross-scan employs four rotationally symmetric scanning paths to respectively process

the four components of the feature map along the group dimension. Formally, given a group-structured 2D feature map  $\mathbf{X} \in \mathbb{R}^{H \times W \times C_1 \times 4}$ , we first partition  $\mathbf{X}$  along the group dimension to get  $[\mathbf{X}^{G_0}, \mathbf{X}^{G_1}, \mathbf{X}^{G_2}, \mathbf{X}^{G_3}]$ . The EQ cross-scan operator  $\tau(\cdot)$  then flattens each group-dimension component  $\mathbf{X}^{G_t}$  into a 1D sequence as follows:

$$\mathbf{x}^{G_t} = \tau_t(\mathbf{X}^{G_t}), \quad \tau_t(\cdot) = \tau_0[\pi_{G_t}^{\mathcal{R}}(\cdot)], \quad (8)$$

where  $\mathbf{x} \in \mathbb{R}^{HW \times C_1 \times 4}$  denotes four resulting 1D feature sequences. Here,  $\tau_0$  represents the base scanning path (corresponding to the standard matrix-to-vector unfolding), and  $\tau_t$  is derived by applying a  $t$  times  $\pi/2$  rotation to  $\tau_0$ .

Symmetrically, we define the inverse operation as EQ-cross-merge  $\tau^{inv}(\cdot)$  for equivariant sequence-to-image reconstruction. That is

$$\mathbf{X}^{G_t} = \tau_t^{inv}(\mathbf{x}^{G_t}), \quad \tau_t^{inv}(\cdot) = \pi_{G_t}^{\mathcal{R}}[\tau_0^{inv}(\cdot)], \quad (9)$$

where  $\tau_0^{inv}$  denotes the standard vector-to-matrix folding. Based on this formulation, we establish the following theoretical guarantees (detailed proofs are provided in the Supplementary Material).

**Theorem 1.** *Let  $\mathbf{X} \in \mathbb{R}^{H \times W \times C \times 4}$  be a group-structured feature map and  $\mathbf{x} \in \mathbb{R}^{HW \times C \times 4}$  be a group-structured feature sequence. Let  $\tau(\cdot)$  and  $\tau^{inv}(\cdot)$  denote the EQ-cross-scan and EQ-cross-merge operators defined in (8) and (9), respectively. For any group element  $G \in \mathcal{G}$ , the following equivariance properties hold:*

$$\tau[\pi_G^{\mathcal{R}S}(\mathbf{X})] = \pi_G^{\mathcal{R}S}[\tau(\mathbf{X})], \quad (10)$$

$$\tau^{inv}[\pi_G^{\mathcal{R}S}(\mathbf{x})] = \pi_G^{\mathcal{R}S}[\tau^{inv}(\mathbf{x})]. \quad (11)$$

Theorem 1 demonstrates that both the EQ-cross-scan  $\tau(\cdot)$  and EQ-cross-merge  $\tau^{inv}(\cdot)$  are strictly equivariant under discrete 90-degree rotations. An intuitive illustration is provided in Fig. 6 (b). When the input image undergoes a  $90^\circ$  spatial rotation and a group-wise cyclic shifting, the resulting 1D sequences generated by EQ-Cross-Scan exhibit only the corresponding channel permutation, thereby ensuring the equivariance of the image-to-sequence flattening process.

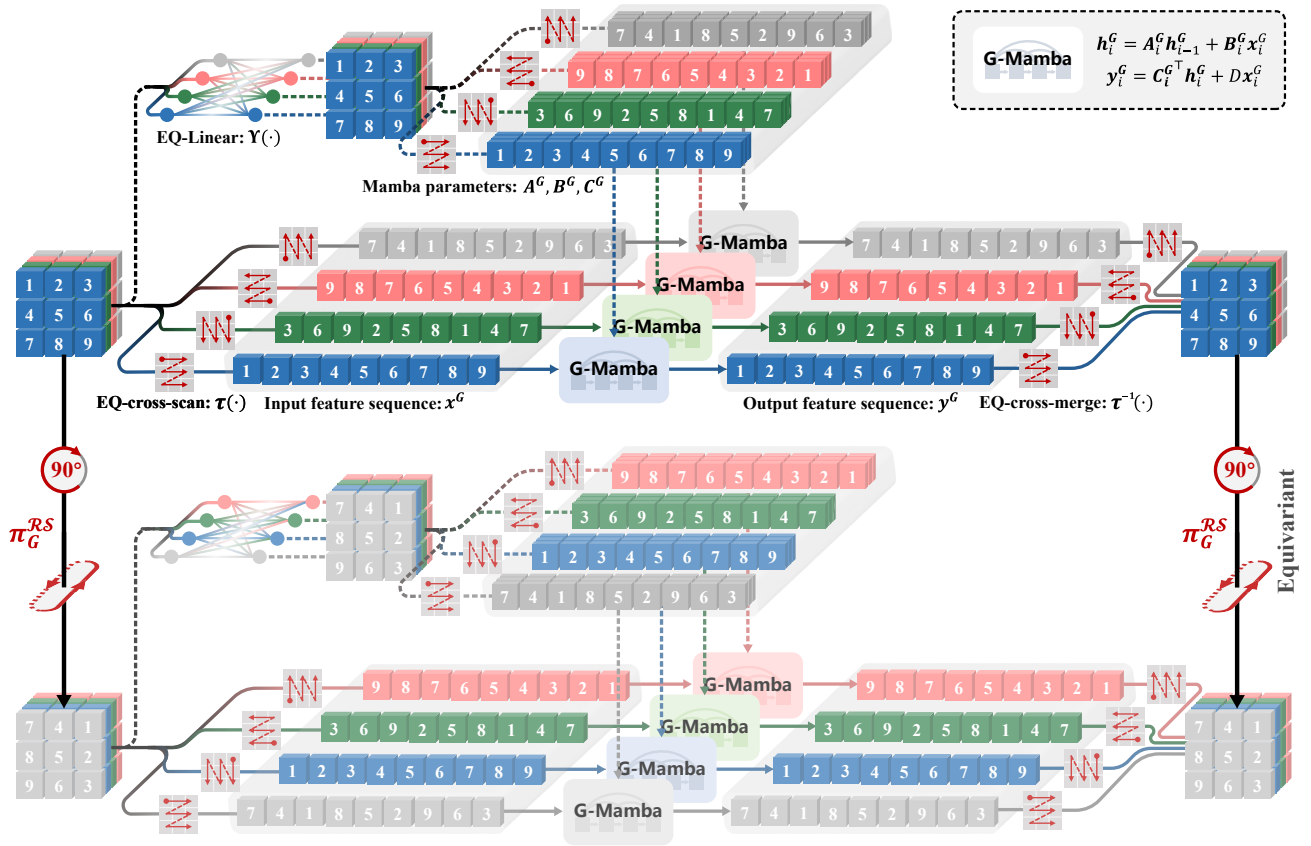


Fig. 7. Architectural pipeline of the proposed equivariant Visual State-Space (EQ-VSS) block. (1) The block first employs EQ-Linear layers to generate input-dependent Mamba parameters  $A_{2D}$ ,  $B_{2D}$ , and  $C_{2D}$ . (2) These parameters, along with the input feature map are partitioned along the group dimension and flattened into four 1D sequences via EQ-cross-scan. (3) Each feature sequence is processed in parallel by the group Mamba block using its corresponding group parameters. (4) Finally, the processed feature map is restored through the EQ-cross-merge operation.

**Group Mamba Blocks.** Following the image-to-sequence flattening process, the vanilla VMamba employs four independent Mamba blocks to process each of the four feature sequences in parallel. However, under rotation transformations, the group-dimensional components of feature maps will be processed by different Mamba blocks compared to the unrotated case, leading to a non-equivariant output. Consequently, the independent parameterization of the Mamba blocks in VMamba lacks rotation equivariance.

To resolve this, we construct the group Mamba blocks by restructuring the learnable parameters  $A$ ,  $B$ , and  $C$  in the Mamba blocks. Specifically, as illustrated in Fig. 7, we first replace the non-equivariant linear layers with EQ-Linear layers  $\Upsilon(\cdot)$  to generate group-structured parameters  $A_{2D}$ ,  $B_{2D}$ , and  $C_{2D}$  from the input 2D feature map  $X \in \mathbb{R}^{H \times W \times C_1 \times 4}$ :

$$A_{2D} = \Upsilon_A(X), \quad B_{2D} = \Upsilon_B(X), \quad C_{2D} = \Upsilon_C(X), \quad (12)$$

where parameters  $A_{2D} \in \mathbb{R}^{H \times W \times C_1 \times N \times 4}$ ,  $B_{2D}$  and  $C_{2D} \in \mathbb{R}^{H \times W \times N \times 4}$ . These parameters are then partitioned into four components along the group dimension and flattened into four 1D parameter sequences using EQ-cross-scan, ensuring structural alignment with the scanned feature sequences:

$$A^{G_t} = \tau_t(A_{2D}^{G_t}), \quad B^{G_t} = \tau_t(B_{2D}^{G_t}), \quad C^{G_t} = \tau_t(C_{2D}^{G_t}), \quad (13)$$

where parameter sequences  $A \in \mathbb{R}^{H \times W \times C_1 \times N \times 4}$ ,  $B$  and  $C \in \mathbb{R}^{H \times W \times N \times 4}$ . These four parameter components, together with a shared scalar parameter  $D$ , are assigned to four parallel

Mamba blocks. Each group Mamba block  $\mathcal{M}(\cdot)$  models its corresponding feature sequences as

$$\begin{aligned} h_i^{G_t} &= A_i^{G_t} h_{i-1}^{G_t} + B_i^{G_t} x_i^{G_t}, \\ y_i^{G_t} &= C_i^{G_t\top} h_i^{G_t} + D x_i^{G_t}, \end{aligned} \quad (14)$$

where  $y \in \mathbb{R}^{H \times W \times C_1 \times 4}$  denotes the output sequences. Finally, the output 2D feature map is restored through EQ-cross-merge, i.e.,  $Y = \tau^{inv}(y)$ . Based on this formulation, we establish the following theoretical guarantees.

**Theorem 2.** *Let  $X \in \mathbb{R}^{H \times W \times C \times T}$  be a group-structured feature map. Given a group Mamba block  $\mathcal{M}(\cdot)$  defined in (14) with parameters  $A$ ,  $B$ , and  $C$  derived according to (12), (13), the following equivariance property holds for any  $G \in \mathcal{G}$ :*

$$\mathcal{M}[\pi_G^S](x, A, B, C, D) = \pi_G^S[\mathcal{M}](x, A, B, C, D), \quad (15)$$

Theorem 2 demonstrates that the proposed group mamba blocks strictly adhere to 90-degree rotation equivariance. Furthermore, by integrating Theorems 1 and 2, we establish that the entire EQ-VSS block is rotationally equivariant. Formally, we derive the following corollary:

**Corollary 1.** *Under the same conditions as Theorem 1 and 2, the EQ-VSS block satisfies the equivariance property for any  $G \in \mathcal{G}$ :*

$$\tau^{inv}[\mathcal{M}][\tau][\pi_G^{RS}](X) = \pi_G^{RS}[\tau^{inv}][\mathcal{M}][\tau](X). \quad (16)$$

Fig. 7 provides an intuitive illustration showing that spatial rotation and group-wise cyclic shifting applied to the input feature map result in identical transformations at the output of EQ-VSS, thereby empirically validating theoretical equivariance property formulated in Corollary 1.

### E. Implementation of Rotation Equivariant Visual Mamba

Leveraging the proposed equivariant modules, we transform two representative Mamba-based architectures, VMamba for high- and mid-level vision tasks and MambaIR for low-level vision tasks, into their equivariant counterparts: EQ-VMamba and EQ-MambaIR. Following these design principles, the proposed formulation can be readily extended to render other Mamba-based visual frameworks end-to-end rotation-equivariant.

**EQ-VMamba for Classification and Segmentation.** For high-level vision tasks, we first construct an EQ-VMamba backbone for feature extraction by following the basic architecture of VMamba [14]. As illustrated in Fig. 5, the EQ-VMamba backbone begins with an EQ-Patch Embedding module, which tokenizes the input image into a group-structured feature map. Subsequently, four network stages are employed to create hierarchical representations. Each stage comprises a stack of EQ-VSS blocks, followed by an EQ-downsampling layer (except for the last stage). Furthermore, all remaining non-equivariant modules—including EQ-depthwise convolution, EQ-LayerNorm2d, and EQ-Dropout—are systematically replaced with their rotation-equivariant variants.

Leveraging the EQ-VMamba backbone for image classification, we employ a simple global average pooling layer to transform the final feature map into the feature vector, followed by an EQ-Linear layer as the classification head, ensuring rotation equivariant predictions. For semantic segmentation, we re-engineer the classical UPerNet [61] decoder into a rotation equivariant variant (EQ-UPerNet) by systematically incorporating EQ-CNN, EQ-Dropout, and EQ-upsampling modules. Following the VMamba protocol, multi-level hierarchical features extracted by the EQ-VMamba backbone are fed into the EQ-UPerNet decoder to produce pixel-wise rotation equivariant segmentation predictions. Finally, we obtain an end-to-end rotation equivariant EQ-VMamba for image classification and segmentation tasks.

**EQ-MambaIR for Image Restoration.** For low-level vision tasks, we develop EQ-MambaIR based on the MambaIR [17] architecture. Most components of MambaIR, such as convolutional layers and VSS blocks, can be directly replaced with their equivariant counterparts. Regarding the reconstruction layers, we replace the original non-equivariant PixelShuffle [62] with an EQ-PixelShuffle module to achieve equivariant upsampling. Additionally, the Channel Attention [63] mechanism used in MambaIR is adapted into a rotation equivariant form by replacing its non-equivariant linear layers with EQ-Linear layers. The resulting EQ-MambaIR framework provides an end-to-end rotation-equivariant solution applicable to a wide array of image restoration tasks.

## IV. EXPERIMENTAL RESULTS

To validate the effectiveness of the proposed framework, we conduct extensive comparative experiments across four representative vision tasks: image classification, semantic segmentation, classical image super-resolution, and lightweight image super-resolution. Beyond standard benchmarks, we further evaluate the classification and segmentation performance of VMamba and EQ-VMamba on rotated datasets to assess their robustness. Furthermore, we perform equivariance verification experiments to empirically measure the equivariance error of EQ-VMamba and EQ-MambaIR. Finally, systematic ablation studies are conducted to validate the necessity of an end-to-end equivariant architecture and the effectiveness of the proposed Group Mamba block.

### A. Image Classification

**Experimental Setting.** We evaluate the classification performance of EQ-VMamba on the ImageNet-100 dataset [66], a widely used subset of ImageNet-1K [67]. ImageNet-100 consists of 100 categories, with 130K images for training and 5K images for validation. Following the training protocol of VMamba [14], all models are trained from scratch using the AdamW optimizer [68] for 300 epochs with a cosine learning rate decay schedule, a batch size of 1024, an initial learning rate of 0.001, and a weight decay of 0.05. To stabilize training, we employ the exponential moving average (EMA) [69] of model parameters. During training, input images are resized to  $224 \times 224$  and employ standard data augmentations, including color jittering, AutoAugment, random erasing, Mixup, and CutMix. Moreover, we develop our EQ-VMamba in two scales: tiny (EQ-VMamba-T) and small (EQ-VMamba-S). For a fair comparison, we reproduce VMamba [14] using the same experimental settings as ours.

**Experimental Results.** Table I presents the comparison results on the ImageNet-100 dataset. EQ-VMamba consistently outperforms the non-equivariant VMamba baseline while utilizing approximately 1/3 of the parameters. Specifically, EQ-VMamba-T achieves a top-1 accuracy of **88.58%**, exceeding VMamba-T by **0.78%** with a parameter reduction from 30M to 10M. Similarly, EQ-VMamba-S achieves **88.70%** top-1 accuracy, outperforming VMamba-S by **0.38%** with a parameter reduction from 50M to 17M. Furthermore, our method also surpasses the rotation invariant Spectral VMamba [34] with fewer learnable parameters. These results demonstrate that the integration of rotation equivariance serves as a powerful inductive bias, boosting performance while significantly enhancing parameter efficiency through group-wise weight sharing.

**Rotated Classification Experimental Results.** Fig. 2 compares the classification robustness of VMamba, Spectral VMamba, and EQ-VMamba under various rotation angles on ImageNet-100. The results show that VMamba exhibits high sensitivity to image rotation, suffering from significant performance degradation. While Spectral VMamba maintains stable performance at cardinal rotations (e.g.,  $0^\circ$ ,  $90^\circ$ ,  $180^\circ$ , and  $270^\circ$ ), its performance drops sharply at intermediate rotation angles. In contrast, EQ-VMamba preserves strict equivariance under 90-degree rotations and demonstrates superior

TABLE I  
QUANTITATIVE COMPARISON OF IMAGE CLASSIFICATION PERFORMANCE ON THE **IMAGENET-100** VALIDATION SET.

Model	Arch.	#Param. (M)	Top-1 (%)	Top-5 (%)	Model	Arch.	#Param. (M)	Top-1 (%)	Top-5 (%)
ConvNeXt-T [6]	CNN	29M	87.06	96.70	ConvNeXt-S [6]	CNN	50M	87.54	96.96
DeiT-S [64]	Trans.	22M	78.88	93.64	DeiT-B [64]	Trans.	86M	78.14	92.60
Swin-T [9]	Trans.	29M	87.42	97.20	Swin-S [9]	Trans.	50M	87.26	97.46
XCiT-S24 [65]	Trans.	26M	87.14	96.98	XCiT-M24 [65]	Trans.	84M	87.72	97.36
Vim-T [13]	SSM	7M	82.20	95.60	Vim-S [13]	SSM	26M	80.24	95.00
MSVMamba-M [42]	SSM	12M	87.56	97.76	MSVMamba-T [42]	SSM	33M	88.44	97.92
SpectralVMamba-T [34]	SSM	21M	87.86	97.25	SpectralVMamba-S [34]	SSM	35M	88.09	97.08
VMamba-T [14]	SSM	30M	87.80	97.70	VMamba-S [14]	SSM	50M	88.32	97.82
EQ-VMamba-T	SSM	<b>10M</b>	<b>88.58</b>	<b>98.14</b>	EQ-VMamba-S	SSM	<b>17M</b>	<b>88.70</b>	<b>98.22</b>

robustness across the entire rotation spectrum. Overall, these results validate that our rotation equivariant design successfully overcomes the robustness bottlenecks of VMamba.

### B. Semantic Segmentation

**Experimental Setting.** We evaluate the semantic segmentation performance of EQ-VMamba on four widely used natural image datasets (ADE20K [70], PASCAL VOC 2012 [71], Cityscapes [72], and COCO-Stuff-164K [73]) and two remote sensing datasets (LoveDA [74] and ISPRS Potsdam). All experiments are implemented using the MMSegmentation [75] framework. For Cityscapes, input images are cropped to  $1024 \times 1024$  with a batch size of 8. For others, input images are cropped to  $512 \times 512$  with a batch size of 16. For natural images, we follow prior work [34] and initialize the EQ-VMamba backbone with ImageNet-100 pretrained weights and adopt EQ-UPerNet as the decoder. All models are trained for 160K iterations using the AdamW optimizer [68] with an initial learning rate of  $6 \times 10^{-5}$ . For remote sensing image segmentation, models are trained from scratch for 15K iterations with an initial learning rate of  $6 \times 10^{-4}$ , following the protocol in Samba [48]. To ensure a fair comparison, all comparison methods are reproduced under the same experimental settings as ours.

**Experimental Results.** Table II summarizes the comparison results across six semantic segmentation datasets. Overall, EQ-VMamba achieves comparable performance to VMamba on natural image datasets while utilizing only approximately 1/4 of the parameters, and substantially outperforms VMamba on remote sensing datasets. Specifically, on natural images, EQ-VMamba-S surpasses VMamba-S on PASCAL VOC 2012, Cityscapes, and COCO-Stuff-164K, though it remains behind on ADE20K. A similar trend is observed for the tiny variants, where EQ-VMamba-T outperforms VMamba-T on two of the four natural image datasets. The advantages of the proposed equivariant VMamba are more pronounced in remote sensing. EQ-VMamba-T significantly exceeds VMamba-S by **3.07%** mIoU on LoveDA and **6.30%** mIoU on ISPRS Potsdam. Moreover, EQ-VMamba-S continues to exceed VMamba-S by **3.14%** mIoU on LoveDA and **5.94%** mIoU on ISPRS Potsdam. Additionally, qualitative visualizations in Fig. 8 demonstrate that EQ-VMamba generates more accurate segmentation predictions than the original VMamba in certain cases.

**Rotated Segmentation Experimental Results.** Table III and Fig. 9 compare the segmentation robustness of

VMamba and EQ-VMamba under cardinal rotations ( $0^\circ, 90^\circ, 180^\circ, 270^\circ$ ) across both natural and remote sensing datasets. Experimental results show that vanilla VMamba suffers substantial performance degradation under rotation on natural images, and marginal degradation on remote sensing images. In contrast, EQ-VMamba demonstrates superior robustness, maintaining nearly constant performance across all datasets. The negligible performance fluctuations observed on specific datasets (e.g., ADE20K) are attributed to irregular test image resolutions rather than a lack of strict architectural equivariance. Specifically, irregular input resolutions lead to subtle differences in patch partitioning after rotation, which can be mitigated by employing zero-padding to standardize input resolutions.

**Analysis of Experimental Results.** Experimental results in Tables II and III reveal a compelling phenomenon: EQ-VMamba achieves substantially larger performance gains on remote sensing datasets compared to natural image datasets. Furthermore, the vanilla VMamba exhibits stronger rotational robustness on remote sensing datasets compared to natural image datasets. We attribute these discrepancies to the intrinsic geometric properties of the dataset. Natural images in these datasets (e.g., ADE20K) typically adhere to canonical "up-right" orientations and lack global rotational symmetry, which restricts the advantages of equivariant architectures. In such cases, the parameter reduction induced by equivariance may slightly constrain model capacity, leading to marginal performance trade-offs. In contrast, remote sensing images—captured from nadir or aerial perspectives—inherently possess stronger rotational symmetry. This allows EQ-VMamba to fully exploit its equivariant inductive bias, resulting in markedly improved performance. These findings underscore that the efficacy of equivariant networks is closely coupled with the underlying symmetry properties of the data distribution.

### C. Classic Image Super-Resolution

**Experimental Setting.** We evaluate the classic image super-resolution (SR) performance of EQ-MambaIR on standard benchmarks with bicubic degradation. Following the training protocol of MambaIR [17], all models are trained on DIV2K [82] and Flickr2K [76] datasets, and evaluated on five widely used datasets: Set5 [83], Set14 [84], B100 [85], Urban100 [86], and Manga109 [87]. During training, we adopt

TABLE II  
QUANTITATIVE COMPARISON OF SEMANTIC SEGMENTATION PERFORMANCE ON NATURAL/REMOTE SENSING IMAGE DATASETS (mIoU: %).

Backbone	#Param. (M)	Natural Image				Remote Sensing Image	
		ADE20K	VOC 2012	Cityscapes	COCO-Stuff	LoveDA	ISPRS Potsdam
ConvNeXt-T [6]	48M	35.59	53.99	76.33	32.81	38.52	50.61
DeiT-S [64]	52M	23.13	24.17	24.29	54.23	38.74	48.63
Swin-T [9]	48M	27.05	35.73	70.05	25.83	40.78	53.78
XCiT-S24 [65]	76M	36.21	58.08	73.02	35.11	36.29	49.01
Vim-T [13]	13M	24.31	32.20	60.04	23.64	36.12	44.01
MSVMamba-M [42]	42M	37.69	59.78	78.40	35.94	41.26	55.34
VMamba-T [14]	62M	<b>40.15</b>	63.70	<b>78.42</b>	38.67	42.62	53.24
EQ-VMamba-T	<b>18M</b>	39.51	<b>64.46</b>	78.01	<b>38.69</b>	<b>45.69</b>	<b>59.54</b>
ConvNeXt-S [6]	70M	36.89	58.83	77.12	35.03	39.01	52.05
DeiT-B [64]	121M	24.43	24.85	56.26	26.40	39.21	50.71
Swin-S [9]	69M	29.19	38.89	73.43	28.20	41.23	54.69
XCiT-M24 [65]	112M	36.39	58.63	73.84	35.75	37.27	50.09
Vim-S [13]	46M	26.62	33.16	63.48	26.91	39.13	50.86
MSVMamba-T [42]	65M	40.70	65.98	78.35	36.63	43.83	57.86
VMamba-S [14]	82M	<b>41.68</b>	66.14	79.03	37.43	40.90	56.06
EQ-VMamba-S	<b>25M</b>	39.90	<b>66.57</b>	<b>80.36</b>	<b>38.30</b>	<b>44.04</b>	<b>62.00</b>

TABLE III  
QUANTITATIVE COMPARISON OF SEMANTIC SEGMENTATION PERFORMANCE ON ROTATED NATURAL/REMOTE SENSING DATASETS (mIoU: %).

Backbone	#Param. (M)	Natural Image				Remote Sensing Image	
		ADE20K	VOC 2012	Cityscapes	COCO-Stuff	LoveDA	ISPRS Potsdam
VMamba-T [14]	62M	15.98 (24.17↓)	40.42 (23.28↓)	32.70 (45.72↓)	24.26 (14.41↓)	41.68 (0.94↓)	53.15 (0.09↓)
EQ-VMamba-T	<b>18M</b>	<b>39.59 (0.08↑)</b>	<b>63.19 (1.27↓)</b>	<b>78.01 (0.00↓)</b>	<b>37.80 (0.50↓)</b>	<b>45.69 (0.00↓)</b>	<b>59.54 (0.00↓)</b>
VMamba-S [14]	82M	19.60 (22.08↓)	47.54 (18.60↓)	39.42 (39.61↓)	26.51 (10.92↓)	39.19 (1.71↓)	53.08 (2.98↓)
EQ-VMamba-S	<b>25M</b>	<b>39.87 (0.03↓)</b>	<b>65.64 (0.93↓)</b>	<b>80.36 (0.00↓)</b>	<b>37.76 (0.54↓)</b>	<b>44.04 (0.00↓)</b>	<b>62.00 (0.00↓)</b>

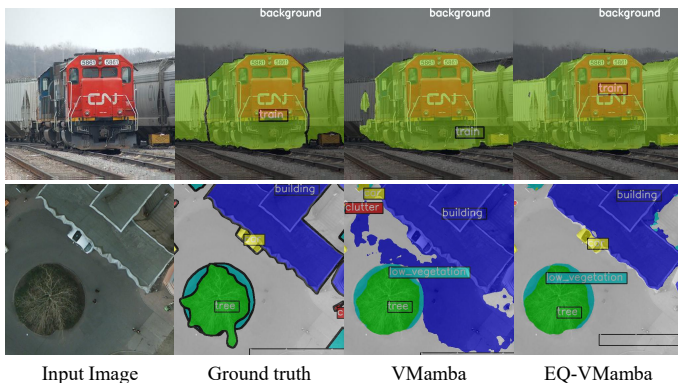


Fig. 8. Visual comparison of segmentation results between VMamba and EQ-VMamba on the PASCAL VOC 2012 natural image dataset (top row) and the ISPRS Potsdam remote sensing dataset (bottom row).

$L_1$  loss function and optimize the network using AdamW [68] with an initial learning rate of  $3 \times 10^{-4}$  and a batch size of 32. The input patch size is set to  $64 \times 64$ . For  $\times 2$  SR, models are trained from scratch for 500K iterations. For  $\times 3$  and  $\times 4$  SR, models are initialized with the pre-trained  $\times 2$  weights and subsequently finetuned for 250K iterations.

**Experimental Results.** Table IV presents the comparison results on standard classic super-resolution benchmarks. The proposed EQ-MambaIR consistently outperforms the MambaIR baseline across all test datasets (Set5, Set14, BSD100, Urban100, and Manga109) and upscaling factors ( $\times 2$ ,  $\times 3$ , and

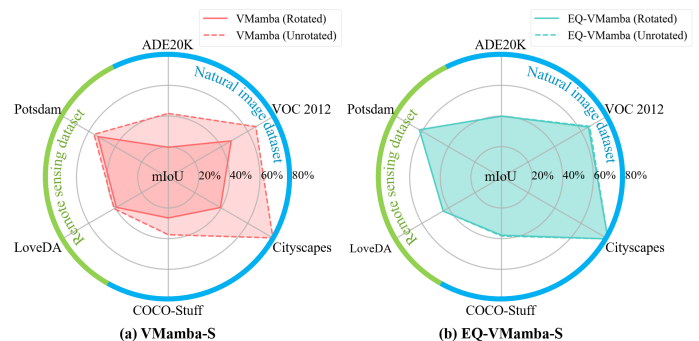


Fig. 9. Robustness comparison of VMamba and EQ-VMamba on the rotated semantic segmentation datasets. Input image rotations lead to a substantial performance degradation in VMamba, while EQ-VMamba preserves performance under 90-degree rotations.

$\times 4$ ). Notably, these performance improvements are achieved while utilizing approximately half the parameters of the original MambaIR. For example, on the challenging Urban100 dataset, EQ-MambaIR (12M parameters) surpasses MambaIR (20M parameters) by **0.17 dB** and **0.13 dB** in PSNR at scales  $\times 2$  and  $\times 3$ , respectively. Similar trends hold across other test datasets, as detailed in the table. Additionally, the visualization results presented in Fig. 10 demonstrate that EQ-MambaIR substantially improves the restoration quality of blurred delicate structures and textual elements in degraded images. These results further underscore the efficacy of integrating rotation

TABLE IV  
QUANTITATIVE COMPARISON OF DIFFERENT METHODS ON THE CLASSIC IMAGE SUPER-RESOLUTION BENCHMARK.

Model	Scale	#Param. (M)	Set5		Set14		BSD100		Urban100		Manga109	
			PSNR	SSIM								
EDSR [76]	×2	42.6M	38.11	0.9602	33.92	0.9195	32.32	0.9013	32.93	0.9351	39.10	0.9773
RCAN [77]	×2	15.4M	38.27	0.9614	34.12	0.9216	32.41	0.9027	33.34	0.9384	39.44	0.9786
SAN [78]	×2	15.7M	38.31	0.9620	34.07	0.9213	32.42	0.9028	33.10	0.9370	39.32	0.9792
HAN [79]	×2	15.9M	38.27	0.9614	34.16	0.9217	32.41	0.9027	33.35	0.9385	39.46	0.9785
IPT [80]	×2	115M	38.37	-	34.43	-	32.48	-	33.76	-	-	-
SwinIR [53]	×2	11.8M	38.42	0.9623	34.46	0.9250	32.53	0.9041	33.81	0.9427	39.92	0.9797
EDT [81]	×2	11.5M	38.45	0.9624	34.57	0.9258	32.52	0.9041	33.80	0.9425	39.93	0.9800
SRFormer [54]	×2	10.4M	38.51	0.9627	34.44	0.9253	32.57	0.9046	34.09	0.9449	40.07	0.9802
MambaIR [17]	×2	20.4M	38.57	0.9627	34.67	0.9261	32.58	0.9048	34.15	0.9446	40.28	0.9806
<b>EQ-MambaIR</b>	<b>×2</b>	<b>12.1M</b>	<b>38.59</b>	<b>0.9629</b>	<b>34.76</b>	<b>0.9268</b>	<b>32.63</b>	<b>0.9056</b>	<b>34.32</b>	<b>0.9458</b>	<b>40.34</b>	<b>0.9810</b>
EDSR [76]	×3	42.6M	34.65	0.9280	30.52	0.8462	29.25	0.8093	28.80	0.8653	34.17	0.9476
RCAN [77]	×3	15.4M	34.74	0.9299	30.65	0.8482	29.32	0.8111	29.09	0.8702	34.44	0.9499
SAN [78]	×3	15.7M	34.75	0.9300	30.59	0.8476	29.33	0.8112	28.93	0.8671	34.30	0.9494
HAN [79]	×3	16.1M	34.75	0.9299	30.67	0.8483	29.32	0.8110	29.10	0.8705	34.48	0.9500
IPT [80]	×3	115M	34.81	-	30.85	-	29.38	-	29.49	-	-	-
SwinIR [53]	×3	11.8M	34.97	0.9318	30.93	0.8534	29.46	0.8145	29.75	0.8826	35.12	0.9537
EDT [81]	×2	11.5M	34.97	0.9316	30.89	0.8527	29.44	0.8142	29.72	0.8814	35.13	0.9534
SRformer [54]	×3	10.6M	35.02	0.9323	30.94	0.8540	29.48	0.8156	30.04	0.8865	35.26	0.9543
MambaIR [17]	×3	20.4M	35.08	0.9323	30.99	0.8536	29.51	0.8157	29.93	0.8841	35.43	0.9546
<b>EQ-MambaIR</b>	<b>×3</b>	<b>12.2M</b>	<b>35.13</b>	<b>0.9327</b>	<b>31.08</b>	<b>0.8546</b>	<b>29.53</b>	<b>0.8170</b>	<b>30.06</b>	<b>0.8869</b>	<b>35.48</b>	<b>0.9550</b>
EDSR [76]	×4	43.0M	32.46	0.8968	28.80	0.7876	27.71	0.7420	26.64	0.8033	31.02	0.9148
RCAN [77]	×4	15.6M	32.63	0.9002	28.87	0.7889	27.77	0.7436	26.82	0.8087	31.22	0.9173
SAN [78]	×4	15.7M	32.64	0.9003	28.92	0.7888	27.78	0.7436	26.79	0.8068	31.18	0.9169
HAN [79]	×4	16.1M	32.64	0.9002	28.90	0.7890	27.80	0.7442	26.85	0.8094	31.42	0.9177
IPT [80]	×4	116M	32.64	-	29.01	-	27.82	-	27.26	-	-	-
SwinIR [53]	×4	11.9M	32.92	0.9044	29.09	0.7950	27.92	0.7489	27.45	0.8254	32.03	0.9260
EDT [81]	×2	11.6M	32.82	0.9031	29.09	0.7939	27.91	0.7483	27.46	0.8246	32.05	0.9254
SRFormer [54]	×4	10.5M	32.93	0.9041	29.08	0.7953	27.94	0.7502	27.68	<b>0.8311</b>	32.21	0.9271
MambaIR [17]	×4	20.4M	33.03	0.9046	29.20	0.7961	<b>27.98</b>	0.7503	27.68	0.8287	32.32	<b>0.9272</b>
<b>EQ-MambaIR</b>	<b>×4</b>	<b>12.2M</b>	<b>33.04</b>	<b>0.9047</b>	<b>29.21</b>	<b>0.7964</b>	<b>27.98</b>	<b>0.7506</b>	<b>27.70</b>	0.8300	<b>32.33</b>	0.9270



Fig. 10. Visual comparison of image super-resolution results between MambaIR and EQ-MambaIR on Urban100 and Manga109 datasets.

symmetry priors into the Mamba framework.

#### D. Lightweight Image Super-Resolution

**Experimental Setting.** For the lightweight image super-resolution task, we evaluate the performance of EQ-MambaIR under stringent capacity constraints. Following the lightweight protocol established in MambaIR [17], we utilize only the DIV2K dataset [82] for training. All other experimental configurations, including optimization and evaluation metrics, remain consistent with the classical SR benchmarks.

**Experimental Results.** Table V presents the comparison results on standard lightweight image super-resolution

benchmarks. EQ-MambaIR-light outperforms the MambaIR-light baseline on most test datasets and upscaling factors, while using significantly fewer parameters. For example, on the challenging Urban100 dataset, EQ-MambaIR-light (519K parameters) significantly surpasses MambaIR-light (859K parameters) by **0.30dB** in PSNR at the ×2 scale, and by **0.10dB** in PSNR at the ×3 and ×4 scales. On the Manga109 dataset, EQ-MambaIR-light still surpasses MambaIR-light by **0.11dB** and **0.09dB** in PSNR at scales ×2 and ×3, respectively. These results further substantiate the advantages of incorporating rotation equivariance into Mamba-based architectures,

TABLE V  
QUANTITATIVE COMPARISON OF DIFFERENT METHODS ON THE LIGHTWEIGHT IMAGE SUPER-RESOLUTION BENCHMARK.

Model	Scale	#Param. (M)	Set5		Set14		BSD100		Urban100		Manga109	
			PSNR	SSIM								
CARN [88]	×2	1,592K	37.76	0.9590	33.52	0.9166	32.09	0.8978	31.92	0.9256	38.36	0.9765
IMDN [89]	×2	694K	38.00	0.9605	33.63	0.9177	32.19	0.8996	32.17	0.9283	38.88	0.9774
LAPAR-A [90]	×2	548K	38.01	0.9605	33.62	0.9183	32.19	0.8999	32.10	0.9283	38.67	0.9772
LatticeNet [91]	×2	756K	38.13	0.9610	33.78	0.9193	32.25	0.9005	32.43	0.9302	-	-
SwinIR-light [53]	×2	910K	38.14	0.9611	33.86	0.9206	32.31	0.9012	32.76	0.9340	39.12	0.9783
ELAN [92]	×2	621K	38.17	0.9611	33.94	0.9207	32.30	0.9012	32.76	0.9340	39.11	0.9782
SRFormer-light [54]	×2	853K	<b>38.23</b>	<b>0.9613</b>	33.94	0.9209	32.36	0.9019	32.91	0.9353	39.28	<b>0.9785</b>
MambaIR-light [17]	×2	859K	38.16	0.9610	<b>34.00</b>	<b>0.9212</b>	32.34	0.9017	32.92	0.9356	39.31	0.9779
EQ-MambaIR-light	×2	<b>519K</b>	38.19	0.9612	33.99	0.9208	<b>32.37</b>	<b>0.9022</b>	<b>33.22</b>	<b>0.9375</b>	<b>39.42</b>	0.9782
CARN [88]	×3	1,592K	34.29	0.9255	30.29	0.8407	29.06	0.8034	28.06	0.8493	33.50	0.9440
IMDN [89]	×3	703K	34.36	0.9270	30.32	0.8417	29.09	0.8046	28.17	0.8519	33.61	0.9445
LAPAR-A [90]	×3	544K	34.36	0.9267	30.34	0.8421	29.11	0.8054	28.15	0.8523	33.51	0.9441
LatticeNet [91]	×3	765K	34.53	0.9281	30.39	0.8424	29.15	0.8059	28.33	0.8538	-	-
SwinIR-light [53]	×3	886K	34.62	0.9289	30.54	0.8463	29.20	0.8082	28.66	0.8624	33.98	0.9478
ELAN [92]	×3	629K	34.61	0.9288	30.55	0.8463	29.21	0.8081	28.69	0.8624	34.00	0.9478
SRFormer-light [54]	×3	861K	34.67	0.9296	30.57	0.8469	29.26	0.8099	28.81	0.8655	34.19	0.9489
MambaIR-light [17]	×3	867K	34.72	0.9296	30.63	0.8475	29.29	0.8099	29.00	0.8689	34.39	0.9495
EQ-MambaIR-light	×3	<b>527K</b>	<b>34.81</b>	<b>0.9302</b>	<b>30.66</b>	<b>0.8483</b>	<b>29.32</b>	<b>0.8105</b>	<b>29.10</b>	<b>0.8708</b>	<b>34.48</b>	<b>0.9499</b>
CARN [88]	×4	1,592K	32.13	0.8937	28.60	0.7806	27.58	0.7349	26.07	0.7837	30.47	0.9084
IMDN [89]	×4	715K	32.21	0.8948	28.58	0.7811	27.56	0.7353	26.04	0.7838	30.45	0.9075
LAPAR-A [90]	×4	659K	32.15	0.8944	28.61	0.7818	27.61	0.7366	26.14	0.7871	30.42	0.9074
LatticeNet [91]	×4	777K	32.30	0.8962	28.68	0.7830	27.62	0.7367	26.25	0.7873	-	-
SwinIR-light [53]	×4	897K	32.44	0.8976	28.77	0.7858	27.69	0.7406	26.47	0.7980	30.92	0.9151
ELAN [92]	×4	640K	32.43	0.8975	28.78	0.7858	27.69	0.7406	26.54	0.7982	30.92	0.9150
SRFormer-light [54]	×4	873K	32.51	0.8988	28.82	0.7872	27.73	0.7422	26.67	0.8032	31.17	0.9165
MambaIR-light [17]	×4	879K	32.51	0.8993	28.85	0.7876	27.75	0.7423	26.75	0.8051	31.26	0.9175
EQ-MambaIR-light	×4	<b>538K</b>	<b>32.70</b>	<b>0.9006</b>	<b>28.89</b>	<b>0.7884</b>	<b>27.78</b>	<b>0.7438</b>	<b>26.85</b>	<b>0.8082</b>	<b>31.31</b>	<b>0.9184</b>

TABLE VI  
AVERAGE EQUIVARIANT ERROR OF DIFFERENT MODELS ON p4 ROTATION GROUP (NMSE ↓).

Model	Image Classification		Semantic Segmentation		Model	Super-Resolution×2		Super-Resolution×4	
	Untrained	Trained	Untrained	Trained		Scratch	Trained	Scratch	Trained
VMamba-T [14]	0.1721	0.4404	0.3547	0.1958	MambaIR [17]	0.1548	0.0050	0.0912	0.0099
EQ-VMamba-T	<b>0.0003</b>	<b>0.0003</b>	<b>0.0004</b>	<b>0.0002</b>	EQ-MambaIR	<b>8.6e-5</b>	<b>0.0004</b>	<b>4.5e-6</b>	<b>0.0001</b>
VMamba-S [14]	0.2017	0.1497	0.3617	0.1809	MambaIR-light [17]	0.4027	0.0061	0.5000	0.0009
EQ-VMamba-S	<b>0.0003</b>	<b>0.0003</b>	<b>0.0004</b>	<b>0.0002</b>	EQ-MambaIR-light	<b>0.0003</b>	<b>0.0004</b>	<b>3.3e-05</b>	<b>6.9e-05</b>

particularly in resource-constrained scenarios where parameter efficiency is paramount.

### E. Equivariance Verification

To empirically verify the theoretical results of equivariance error presented in Sec. III, we further conduct experiments to quantitatively evaluate the equivariance errors of EQ-VMamba and EQ-MambaIR relative to their non-equivariant counterparts under the p4 rotation group.

**Experimental Setting.** Following the equivariance evaluation protocol established in [32], we measure equivariance by comparing the model’s predictions to transformed inputs. Specifically, for an input image  $I$  and a rotation transformation  $\pi_G^S$  sampled from the p4 group (i.e.,  $\{0^\circ, 90^\circ, 180^\circ, 270^\circ\}$ ), we feed both  $I$  and its rotated version  $\pi_G^S(I)$  into the model  $\mathcal{F}(\cdot)$  to obtain their respective outputs. We utilize the Normalized Mean Squared Error (NMSE) between  $\mathcal{F}[\pi_G^S](I)$  and  $\pi_G^S[\mathcal{F}](I)$  as the quantitative metric for equivariance error. For high-level and mid-level vision tasks, we compare the

equivariance errors of VMamba and EQ-VMamba on the ImageNet-100 and ADE20K test datasets. For low-level vision tasks, we compare the equivariance errors of MambaIR and EQ-MambaIR on the Urban100 dataset for ×2 and ×4 image super-resolution. Notably, as our architecture’s equivariance is an inherent structural attribute rather than a learned property, we report errors for both randomly initialized (untrained) and fully converged (trained) models to highlight this training-free characteristic.

**Experimental Results.** Table VI summarizes the average equivariant error of different models on p4 rotation group. Notably, the equivariance errors of EQ-VMamba and EQ-MambaIR are negligible—effectively approaching zero across all settings—and are several orders of magnitude lower than those of their non-equivariant baselines. These results empirically validate that EQ-VMamba and EQ-MambaIR achieve robust end-to-end rotation equivariance. Consistent with prior observations in [32], the measured equivariance error is not exactly zero in practice. This residual error is attributed to

TABLE VII  
ABLATION STUDY ON EQ-CROSS-SCAN AND EQ-VSS BLOCK.

EQ-cross scan	EQ-VSS block	Model scale	#Param. (M)	Top-1 (%)	Top-5 (%)
$\times$	$\times$	Tiny	30M	87.80	97.70
$\checkmark$	$\times$	Tiny	30M	87.88	97.54
$\checkmark$	$\checkmark$	Tiny	10M	<b>88.58</b>	<b>98.14</b>
$\times$	$\times$	Small	50M	88.32	97.82
$\checkmark$	$\times$	Small	50M	87.76	97.70
$\checkmark$	$\checkmark$	Small	17M	<b>88.70</b>	<b>98.22</b>

TABLE VIII  
ABLATION STUDY ON THE GROUP MAMBA BLOCK.

Mamba block type	Model scale	#Param. (M)	Top-1 (%)	Top-5 (%)
Independent Mamba block	Tiny	9M	87.98	97.96
Group Mamba block	Tiny	10M	<b>88.58</b>	<b>98.14</b>
Independent Mamba block	Small	15M	88.04	97.98
Group Mamba block	Small	17M	<b>88.70</b>	<b>98.22</b>

floating-point numerical precision limits within the PyTorch implementations rather than architectural deficiencies. Overall, these empirical findings are in strict alignment with our theoretical derivations.

#### F. Ablation Study

**Effectiveness of Equivariant Modules.** To validate the necessity of constructing an end-to-end equivariant architecture, we perform an ablation study on the EQ-cross-scan and EQ-VSS blocks. Specifically, we progressively replace the vanilla cross-scan and VSS blocks in the baseline Mamba with their equivariant counterparts and evaluate the impact on ImageNet-100. As shown in Table VII, employing EQ-cross-scan in isolation yields negligible performance improvements. Significant improvements are only realized when all non-equivariant modules are replaced with their equivariant counterparts, ensuring strict end-to-end rotation equivariance.

**Effectiveness of the Group Mamba block.** To verify the necessity of feature interaction across the group dimension, we conduct an ablation study on ImageNet-100 by only replacing all group Mamba blocks in EQ-VMamba-T and EQ-VMamba-S with "independent" Mamba blocks. Specifically, the independent variant employs standard shared linear layers instead of our EQ-Linear layers to generate the parameters  $A$ ,  $B$ , and  $C$ . While maintaining equivariance, this independent variant lacks inter-group feature interaction. As shown in Table VIII, the group Mamba block significantly outperforms the independent variant, yielding Top-1 accuracy improvements of **0.58%** (tiny) and **0.72%** (small), respectively. These improvements demonstrate that integrating features across the group dimension provides a more effective inductive bias than independent processing of group components.

## V. CONCLUSION

In this paper, we have introduced EQ-VMamba, the first rotation equivariant Mamba-based architecture designed for vision tasks. Driven by the observed sensitivity of the vanilla

VMamba to image rotations, we successfully incorporate rotation equivariance into the Mamba framework through two core innovations: a rotation equivariant cross-scan strategy and the group Mamba block. We provide a rigorous theoretical derivation to substantiate that the proposed framework ensures strict end-to-end 90-degree rotation equivariance. Extensive experiments across multiple benchmarks—including high-level image classification task, mid-level semantic segmentation task, and low-level image super-resolution—demonstrate that EQ-VMamba consistently outperforms the baseline VMamba, achieving superior accuracy, enhanced robustness, and significantly reduced equivariance error.

The current EQ-VMamba focuses on the 90-degree rotation group (i.e., the  $p4$  group). A natural extension for future research is to generalize this framework to higher-order rotation groups (e.g.,  $p8$ ) or reflection groups to further bolster the model's equivariant capabilities. Another promising direction is the development of quantitative metric for dataset-level symmetries. Our experimental observations in Sec. IV-B suggest that the efficacy of equivariant networks is closely coupled with the symmetry properties of the data distribution. Establishing a formal mathematical measure of dataset symmetry could provide a more principled guide for estimating the potential gains of equivariant architectures. Furthermore, given that EQ-VMamba utilizes cyclic parameter sharing within its EQ-Linear layers, exploring hardware-aware acceleration for EQ-Linear remains a critical direction to fully leverage the linear-complexity efficiency of the Mamba framework.

## REFERENCES

- [1] Albert Gu and Tri Dao. Mamba: Linear-time sequence modeling with selective state spaces. In *First conference on language modeling*, 2024.
- [2] Karen Simonyan and Andrew Zisserman. Very deep convolutional networks for large-scale image recognition. *arXiv preprint arXiv:1409.1556*, 2014.
- [3] Kaiming He, Xiangyu Zhang, Shaoqing Ren, and Sun Jian. Deep residual learning for image recognition. In *Proceedings of the IEEE/CVF conference on computer vision and pattern recognition*, 2016.
- [4] Gao Huang, Zhuang Liu, Laurens Van Der Maaten, and Kilian Q Weinberger. Densely connected convolutional networks. In *Proceedings of the IEEE/CVF conference on computer vision and pattern recognition*, pages 4700–4708, 2017.
- [5] Mingxing Tan and Quoc Le. Efficientnet: Rethinking model scaling for convolutional neural networks. In *International conference on machine learning*, pages 6105–6114. PMLR, 2019.
- [6] Zhuang Liu, Hanzi Mao, Chao-Yuan Wu, Christoph Feichtenhofer, Trevor Darrell, and Saining Xie. A convnet for the 2020s. In *Proceedings of the IEEE/CVF conference on computer vision and pattern recognition*, pages 11976–11986, 2022.
- [7] Ashish Vaswani, Noam Shazeer, Niki Parmar, Jakob Uszkoreit, Llion Jones, Aidan N Gomez, Łukasz Kaiser, and Illia Polosukhin. Attention is all you need. *Advances in neural information processing systems*, 30, 2017.
- [8] Alexey Dosovitskiy, Lucas Beyer, Alexander Kolesnikov, et al. An image is worth 16x16 words: Transformers for image recognition at scale. In *The Tenth International Conference on Learning Representations*, 2021.
- [9] Ze Liu, Yutong Lin, Yue Cao, Han Hu, Yixuan Wei, Zheng Zhang, Stephen Lin, and Baining Guo. Swin transformer: Hierarchical vision transformer using shifted windows. In *Proceedings of the IEEE/CVF international conference on computer vision*, pages 10012–10022, 2021.
- [10] Albert Gu, Isys Johnson, Karan Goel, Khaled Saab, Tri Dao, Atri Rudra, and Christopher Ré. Combining recurrent, convolutional, and continuous-time models with linear state space layers. *Advances in neural information processing systems*, 34:572–585, 2021.
- [11] Albert Gu, Karan Goel, and Christopher Ré. Efficiently modeling long sequences with structured state spaces. *arXiv preprint arXiv:2111.00396*, 2021.

- [12] Jimmy TH Smith, Andrew Warrington, and Scott W Linderman. Simplified state space layers for sequence modeling. *arXiv preprint arXiv:2208.04933*, 2022.
- [13] Lianghui Zhu, Bencheng Liao, Qian Zhang, Xinlong Wang, Wenyu Liu, and Xinggang Wang. Vision mamba: Efficient visual representation learning with bidirectional state space model. *arXiv preprint arXiv:2401.09417*, 2024.
- [14] Yue Liu, Yunjie Tian, Yuzhong Zhao, Hongtian Yu, Lingxi Xie, Yaowei Wang, Qixiang Ye, Jianbin Jiao, and Yunfan Liu. Vmamba: Visual state space model. In *Advances in Neural Information Processing Systems*, pages 103031–103063, 2024.
- [15] Chaodong Xiao, Minghan Li, Zhengqiang Zhang, Deyu Meng, and Lei Zhang. Spatial-mamba: Effective visual state space models via structure-aware state fusion. In *The Fourteenth International Conference on Learning Representations*, 2025.
- [16] Zhongchen Zhao, Chaodong Xiao, Hui Lin, Qi Xie, Lei Zhang, and Deyu Meng. Polyline path masked attention for vision transformer. *arXiv preprint arXiv:2506.15940*, 2025.
- [17] Hang Guo, Jinmin Li, Tao Dai, Zhihao Ouyang, Xudong Ren, and Shu-Tao Xia. Mambair: A simple baseline for image restoration with state-space model. In *European conference on computer vision*, pages 222–241. Springer, 2024.
- [18] Matthew D Zeiler and Rob Fergus. Visualizing and understanding convolutional networks. In *European conference on computer vision*, pages 818–833. Springer, 2014.
- [19] Taco Cohen and Max Welling. Group equivariant convolutional networks. In *International conference on machine learning*, pages 2990–2999. PMLR, 2016.
- [20] Maurice Weiler and Gabriele Cesa. General  $e(2)$ -equivariant steerable cnns. *Advances in neural information processing systems*, 32, 2019.
- [21] Zhengyang Shen, Lingshen He, Zhouchen Lin, and Jinwen Ma. Pdoconv: Partial differential operator based equivariant convolutions. In *International Conference on Machine Learning*, pages 8697–8706. PMLR, 2020.
- [22] Qi Xie, Qian Zhao, Zongben Xu, and Deyu Meng. Fourier series expansion based filter parametrization for equivariant convolutions. *IEEE Transactions on Pattern Analysis and Machine Intelligence*, 45(4):4537–4551, 2022.
- [23] Lingshen He, Yuxuan Chen, Yiming Dong, Yisen Wang, Zhouchen Lin, et al. Efficient equivariant network. *Advances in Neural Information Processing Systems*, 34:5290–5302, 2021.
- [24] Renjun Xu, Kaifan Yang, Ke Liu, and Fengxiang He.  $e(2)$ -equivariant vision transformer. In *Uncertainty in Artificial Intelligence*, pages 2356–2366. PMLR, 2023.
- [25] Soumyabrata Kundu and Risi Kondor. Steerable transformers for volumetric data. *arXiv preprint arXiv:2405.15932*, 2024.
- [26] Taco S Cohen and Max Welling. Steerable cnns. *arXiv preprint arXiv:1612.08498*, 2016.
- [27] Daniel E Worrall, Stephan J Garbin, Daniyar Turmukhambetov, and Gabriel J Brostow. Harmonic networks: Deep translation and rotation equivariance. In *Proceedings of the IEEE conference on computer vision and pattern recognition*, pages 5028–5037, 2017.
- [28] Yanzhao Zhou, Qixiang Ye, Qiang Qiu, and Jianbin Jiao. Oriented response networks. In *Proceedings of the IEEE Conference on Computer Vision and Pattern Recognition*, pages 519–528, 2017.
- [29] Diego Marcos, Michele Volpi, Nikos Komodakis, and Devis Tuia. Rotation equivariant vector field networks. In *Proceedings of the IEEE International Conference on Computer Vision*, pages 5048–5057, 2017.
- [30] Maurice Weiler, Fred A Hamprecht, and Martin Storath. Learning steerable filters for rotation equivariant cnns. In *Proceedings of the IEEE Conference on Computer Vision and Pattern Recognition*, pages 849–858, 2018.
- [31] David W Romero and Jean-Baptiste Cordonnier. Group equivariant stand-alone self-attention for vision. *arXiv preprint arXiv:2010.00977*, 2020.
- [32] Qi Xie, Jiahong Fu, Zongben Xu, and Deyu Meng. Rotation equivariant arbitrary-scale image super-resolution. *arXiv preprint arXiv:2508.05160*, 2025.
- [33] Yulu Bai, Jiahong Fu, Qi Xie, and Deyu Meng. A regularization-guided equivariant approach for image restoration. In *Proceedings of the Computer Vision and Pattern Recognition Conference*, pages 2300–2310, 2025.
- [34] Sahar Dastani, Ali Bahri, Moslem Yazdanpanah, Mehrdad Noori, David Osowiecki, Gustavo Adolfo Vargas Hakim, Farzad Beizae, Milad Cheraghilkhani, Arnab Kumar Mondal, Herve Lombaert, et al. Spectral state space model for rotation-invariant visual representation learning. In *Proceedings of the Computer Vision and Pattern Recognition Conference*, pages 23881–23890, 2025.
- [35] Michael J Hutchinson, Charline Le Lan, Sheheryar Zaidi, Emilien Dupont, Yee Whye Teh, and Hyunjik Kim. Lietransformer: Equivariant self-attention for lie groups. In *International conference on machine learning*, pages 4533–4543. PMLR, 2021.
- [36] Angelos Katharopoulos, Apoorv Vyas, Nikolaos Pappas, and François Fleuret. Transformers are rnns: Fast autoregressive transformers with linear attention. In *International conference on machine learning*, pages 5156–5165. PMLR, 2020.
- [37] Rewon Child. Generating long sequences with sparse transformers. *arXiv preprint arXiv:1904.10509*, 2019.
- [38] Sepp Hochreiter and Jürgen Schmidhuber. Long short-term memory. *Neural computation*, 9(8):1735–1780, 1997.
- [39] Bo Peng, Eric Alcaide, Quentin Anthony, Alon Albalak, Samuel Arcadinho, Stella Biderman, Huanqi Cao, Xin Cheng, Michael Chung, Matteo Grella, et al. Rkv: Reinventing rnns for the transformer era. *arXiv preprint arXiv:2305.13048*, 2023.
- [40] Yutao Sun, Li Dong, Shaohan Huang, Shuming Ma, Yuqing Xia, Jilong Xue, Jianyong Wang, and Furu Wei. Retentive network: A successor to transformer for large language models. *arXiv preprint arXiv:2307.08621*, 2023.
- [41] Tao Huang, Xiaohuan Pei, Shan You, Fei Wang, Chen Qian, and Chang Xu. Localmamba: Visual state space model with windowed selective scan. In *European Conference on Computer Vision*, pages 12–22. Springer, 2024.
- [42] Yuheng Shi, Minjing Dong, and Chang Xu. Multi-scale vmamba: Hierarchy in hierarchy visual state space model. *Advances in Neural Information Processing Systems*, 37:25687–25708, 2024.
- [43] Dongchen Han, Ziyi Wang, Zhuofan Xia, Yizeng Han, Yifan Pu, Chunjiang Ge, Jun Song, Shiji Song, Bo Zheng, and Gao Huang. Demystify mamba in vision: A linear attention perspective. *Advances in neural information processing systems*, 37:127181–127203, 2024.
- [44] Hang Guo, Yong Guo, Yaohua Zha, Yulun Zhang, Wenbo Li, Tao Dai, Shu-Tao Xia, and Yawei Li. Mambairv2: Attentive state space restoration. *arXiv preprint arXiv:2411.15269*, 2024.
- [45] Zhen Zou, Hu Yu, Jie Huang, and Feng Zhao. Freqmamba: Viewing mamba from a frequency perspective for image deraining. In *Proceedings of the 32nd ACM international conference on multimedia*, pages 1905–1914, 2024.
- [46] Yao Teng, Yue Wu, Han Shi, Xuefei Ning, Guohao Dai, Yu Wang, Zhenguo Li, and Xihui Liu. Dim: Diffusion mamba for efficient high-resolution image synthesis. *arXiv preprint arXiv:2405.14224*, 2024.
- [47] Kunchang Li, Xinhao Li, Yi Wang, Yinan He, Yali Wang, Limin Wang, and Yu Qiao. Videomamba: State space model for efficient video understanding. In *European conference on computer vision*, pages 237–255. Springer, 2024.
- [48] Qinfeng Zhu, Yuanzhi Cai, Yuan Fang, Yihan Yang, Cheng Chen, Lei Fan, and Anh Nguyen. Samba: Semantic segmentation of remotely sensed images with state space model. *Heliyon*, 10(19), 2024.
- [49] Sijie Zhao, Hao Chen, Xueliang Zhang, Pengfeng Xiao, Lei Bai, and Wanli Ouyang. Rs-mamba for large remote sensing image dense prediction. *IEEE Transactions on Geoscience and Remote Sensing*, 2024.
- [50] Dingkan Liang, Xin Zhou, Wei Xu, Xingkui Zhu, Zhikang Zou, Xiaoqing Ye, Xiao Tan, and Xiang Bai. Pointmamba: A simple state space model for point cloud analysis. *Advances in neural information processing systems*, 37:32653–32677, 2024.
- [51] Guowen Zhang, Lue Fan, Chenhang He, Zhen Lei, Zhaoxiang Zhang, and Lei Zhang. Voxel mamba: Group-free state space models for point cloud based 3d object detection. *Advances in Neural Information Processing Systems*, 37:81489–81509, 2024.
- [52] Jiacheng Ruan, Jincheng Li, and Suncheng Xiang. Vm-unet: Vision mamba unet for medical image segmentation. *ACM Transactions on Multimedia Computing, Communications and Applications*, 2024.
- [53] Jingyun Liang, Jiezhong Cao, Guolei Sun, Kai Zhang, Luc Van Gool, and Radu Timofte. Swinir: Image restoration using swin transformer. In *Proceedings of the IEEE/CVF international conference on computer vision*, pages 1833–1844, 2021.
- [54] Yupeng Zhou, Zhen Li, Chun-Le Guo, Song Bai, Ming-Ming Cheng, and Qibin Hou. Srformer: Permuted self-attention for single image super-resolution. In *Proceedings of the IEEE/CVF international conference on computer vision*, pages 12780–12791, 2023.
- [55] Dmitry Laptev, Nikolay Savinov, Joachim M Buhmann, and Marc Pollefeys. Ti-pooling: transformation-invariant pooling for feature learning in convolutional neural networks. In *Proceedings of the IEEE conference on computer vision and pattern recognition*, pages 289–297, 2016.

- [56] Kihyuk Sohn and Honglak Lee. Learning invariant representations with local transformations. *arXiv preprint arXiv:1206.6418*, 2012.
- [57] Alex Krizhevsky, Ilya Sutskever, and Geoffrey E Hinton. Imagenet classification with deep convolutional neural networks. *Advances in neural information processing systems*, 25, 2012.
- [58] Emiel Hoogeboom, Jörn WT Peters, Taco S Cohen, and Max Welling. Hexaconv. *arXiv preprint arXiv:1803.02108*, 2018.
- [59] Zhengyang Shen, Tiancheng Shen, Zhouchen Lin, and Jinwen Ma. Pdoes2cnns: Partial differential operator based equivariant spherical cnns. In *Proceedings of the AAAI conference on artificial intelligence*, volume 35, pages 9585–9593, 2021.
- [60] Siamak Ravanbakhsh. Universal equivariant multilayer perceptrons. In *International Conference on Machine Learning*, pages 7996–8006. PMLR, 2020.
- [61] Tete Xiao, Yingcheng Liu, Bolei Zhou, Yuning Jiang, and Jian Sun. Unified perceptual parsing for scene understanding. In *Proceedings of the European conference on computer vision (ECCV)*, pages 418–434, 2018.
- [62] Wenzhe Shi, Jose Caballero, Ferenc Huszár, Johannes Totz, Andrew P Aitken, Rob Bishop, Daniel Rueckert, and Zehan Wang. Real-time single image and video super-resolution using an efficient sub-pixel convolutional neural network. In *Proceedings of the IEEE conference on computer vision and pattern recognition*, pages 1874–1883, 2016.
- [63] Jie Hu, Li Shen, and Gang Sun. Squeeze-and-excitation networks. In *Proceedings of the IEEE conference on computer vision and pattern recognition*, pages 7132–7141, 2018.
- [64] Hugo Touvron, Matthieu Cord, Matthijs Douze, Francisco Massa, Alexandre Sablayrolles, and Hervé Jégou. Training data-efficient image transformers & distillation through attention. In *International conference on machine learning*, pages 10347–10357. PMLR, 2021.
- [65] Alaaeldin Ali, Hugo Touvron, Mathilde Caron, Piotr Bojanowski, Matthijs Douze, Armand Joulin, Ivan Laptev, Natalia Neverova, Gabriel Synnaeve, Jakob Verbeek, et al. Xcit: Cross-covariance image transformers. *Advances in neural information processing systems*, 34:20014–20027, 2021.
- [66] ambityga (Kaggle user). Imagenet100 (kaggle dataset). <https://www.kaggle.com/datasets/ambityga/imagenet100>, 2023. Accessed: 2025-04-21.
- [67] Jia Deng, Wei Dong, Richard Socher, et al. Imagenet: A large-scale hierarchical image database. In *Proceedings of the IEEE/CVF conference on computer vision and pattern recognition*, 2009.
- [68] Ilya Loshchilov and Frank Hutter. Decoupled weight decay regularization. *arXiv preprint arXiv:1711.05101*, 2017.
- [69] Boris T Polyak and Anatoli B Juditsky. Acceleration of stochastic approximation by averaging. *SIAM journal on control and optimization*, 30(4):838–855, 1992.
- [70] Bolei Zhou, Hang Zhao, Xavier Puig, et al. Scene parsing through ade20k dataset. In *Proceedings of the IEEE/CVF conference on computer vision and pattern recognition*, 2017.
- [71] Mark Everingham, Luc Van Gool, Christopher KI Williams, John Winn, and Andrew Zisserman. The pascal visual object classes (voc) challenge. *International journal of computer vision*, 88(2):303–338, 2010.
- [72] Marius Cordts, Mohamed Omran, Sebastian Ramos, Timo Rehfeld, Markus Enzweiler, Rodrigo Benenson, Uwe Franke, Stefan Roth, and Bernt Schiele. The cityscapes dataset for semantic urban scene understanding. In *Proceedings of the IEEE conference on computer vision and pattern recognition*, pages 3213–3223, 2016.
- [73] Holger Caesar, Jasper Uijlings, and Vittorio Ferrari. Coco-stuff: Thing and stuff classes in context. In *Proceedings of the IEEE conference on computer vision and pattern recognition*, pages 1209–1218, 2018.
- [74] Junjue Wang, Zhuo Zheng, Ailong Ma, Xiaoyan Lu, and Yanfei Zhong. Loveda: A remote sensing land-cover dataset for domain adaptive semantic segmentation. *arXiv preprint arXiv:2110.08733*, 2021.
- [75] MMSegmentation Contributors. Mmssegmentation, an open source semantic segmentation toolbox, 2020.
- [76] Bee Lim, Sanghyun Son, Heewon Kim, Seungjun Nah, and Kyoung Mu Lee. Enhanced deep residual networks for single image super-resolution. In *Proceedings of the IEEE conference on computer vision and pattern recognition workshops*, pages 136–144, 2017.
- [77] Yulun Zhang, Kungpeng Li, Kai Li, Lichen Wang, Bineng Zhong, and Yun Fu. Image super-resolution using very deep residual channel attention networks. In *Proceedings of the European conference on computer vision (ECCV)*, pages 286–301, 2018.
- [78] Tao Dai, Jianrui Cai, Yongbing Zhang, Shu-Tao Xia, and Lei Zhang. Second-order attention network for single image super-resolution. In *Proceedings of the IEEE/CVF conference on computer vision and pattern recognition*, pages 11065–11074, 2019.
- [79] Ben Niu, Weilei Wen, Wenqi Ren, Xiangde Zhang, Lianping Yang, Shuzhen Wang, Kaihao Zhang, Xiaochun Cao, and Haifeng Shen. Single image super-resolution via a holistic attention network. In *European conference on computer vision*, pages 191–207. Springer, 2020.
- [80] Hanqing Chen, Yunhe Wang, Tianyu Guo, Chang Xu, Yiping Deng, Zhenhua Liu, Siwei Ma, Chunjing Xu, Chao Xu, and Wen Gao. Pre-trained image processing transformer. In *Proceedings of the IEEE/CVF conference on computer vision and pattern recognition*, pages 12299–12310, 2021.
- [81] Wenbo Li, Xin Lu, Shengju Qian, Jiangbo Lu, Xiangyu Zhang, and Jiaya Jia. On efficient transformer-based image pre-training for low-level vision. *arXiv preprint arXiv:2112.10175*, 2021.
- [82] Radu Timofte, Eirikur Agustsson, Luc Van Gool, Ming-Hsuan Yang, and Lei Zhang. Ntire 2017 challenge on single image super-resolution: Methods and results. In *Proceedings of the IEEE conference on computer vision and pattern recognition workshops*, pages 114–125, 2017.
- [83] Marco Bevilacqua, Aline Roumy, Christine Guillemot, and Marie Line Alberi-Morel. Low-complexity single-image super-resolution based on nonnegative neighbor embedding. 2012.
- [84] Roman Zeyde, Michael Elad, and Matan Protter. On single image scale-up using sparse-representations. In *Curves and Surfaces: 7th International Conference, Avignon, France, June 24-30, 2010, Revised Selected Papers 7*, pages 711–730. Springer, 2012.
- [85] David Martin, Charless Fowlkes, Doron Tal, and Jitendra Malik. A database of human segmented natural images and its application to evaluating segmentation algorithms and measuring ecological statistics. In *Proceedings Eighth IEEE International Conference on Computer Vision. ICCV 2001*, volume 2, pages 416–423. IEEE, 2001.
- [86] Jia-Bin Huang, Abhishek Singh, and Narendra Ahuja. Single image super-resolution from transformed self-exemplars. In *Proceedings of the IEEE conference on computer vision and pattern recognition*, pages 5197–5206, 2015.
- [87] Yusuke Matsui, Kota Ito, Yuji Aramaki, Azuma Fujimoto, Toru Ogawa, Toshihiko Yamasaki, and Kiyoharu Aizawa. Sketch-based manga retrieval using manga109 dataset. *Multimedia Tools and Applications*, 76:21811–21838, 2017.
- [88] Namhyuk Ahn, Byungkon Kang, and Kyung-Ah Sohn. Fast, accurate, and lightweight super-resolution with cascading residual network. In *Proceedings of the European conference on computer vision (ECCV)*, pages 252–268, 2018.
- [89] Zheng Hui, Xinbo Gao, Yunchu Yang, and Xiumei Wang. Lightweight image super-resolution with information multi-distillation network. In *Proceedings of the 27th acm international conference on multimedia*, pages 2024–2032, 2019.
- [90] Wenbo Li, Kun Zhou, Lu Qi, Nianjuan Jiang, Jiangbo Lu, and Jiaya Jia. Lapar: Linearly-assembled pixel-adaptive regression network for single image super-resolution and beyond. *Advances in Neural Information Processing Systems*, 33:20343–20355, 2020.
- [91] Xiaotong Luo, Yuan Xie, Yulun Zhang, Yanyun Qu, Cuihua Li, and Yun Fu. Latticenet: Towards lightweight image super-resolution with lattice block. In *Computer Vision—ECCV 2020: 16th European Conference, Glasgow, UK, August 23–28, 2020, Proceedings, Part XXII 16*, pages 272–289. Springer, 2020.
- [92] Xindong Zhang, Hui Zeng, Shi Guo, and Lei Zhang. Efficient long-range attention network for image super-resolution. In *European conference on computer vision*, pages 649–667. Springer, 2022.